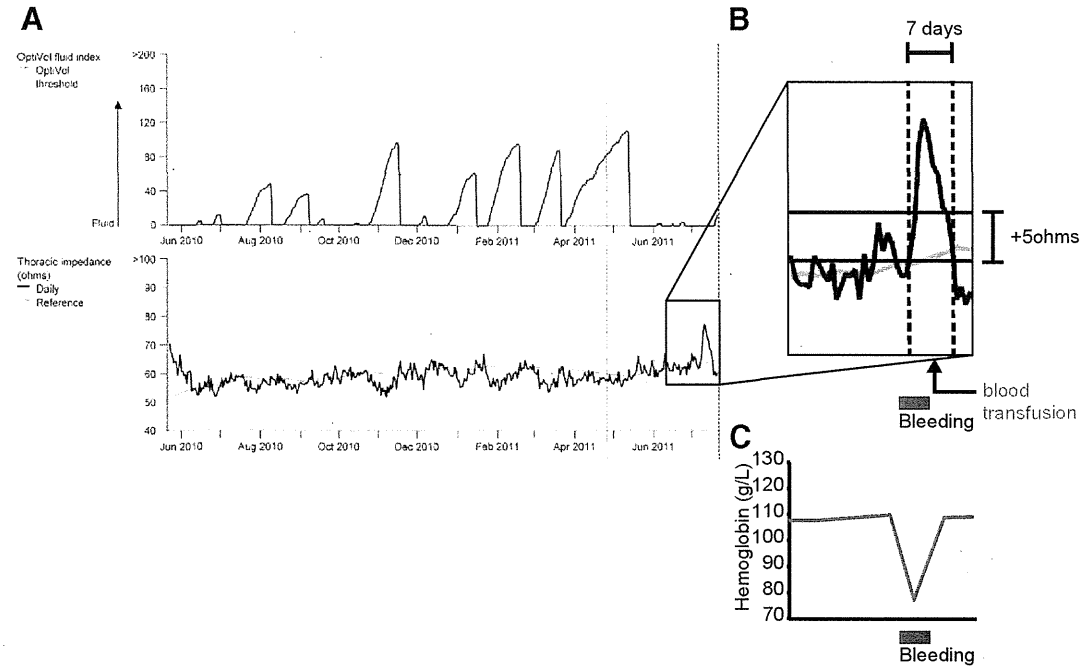

Figure 4. Typical large positive deviation of thoracic impedance (PDI) in intrathoracic impedance in the bleeding event during treatment of chronic heart failure patients. The OptiVol fluid trends report presents up to 14 months of rolling information on the patient's OptiVol fluid index, average daily impedance and reference impedance (**A**,**B**). The time-course of intrathoracic impedance during gastrointestinal bleeding and anemia (Bleeding: closed box) is shown (**B**). A large PDI was recorded consistent with the period of bleeding and blood transfusion. After resolution of the anemia, the large PDI disappeared (**B**). The time-course of hemoglobin concentration over the same periods in **Figure 3B** is shown (**C**).

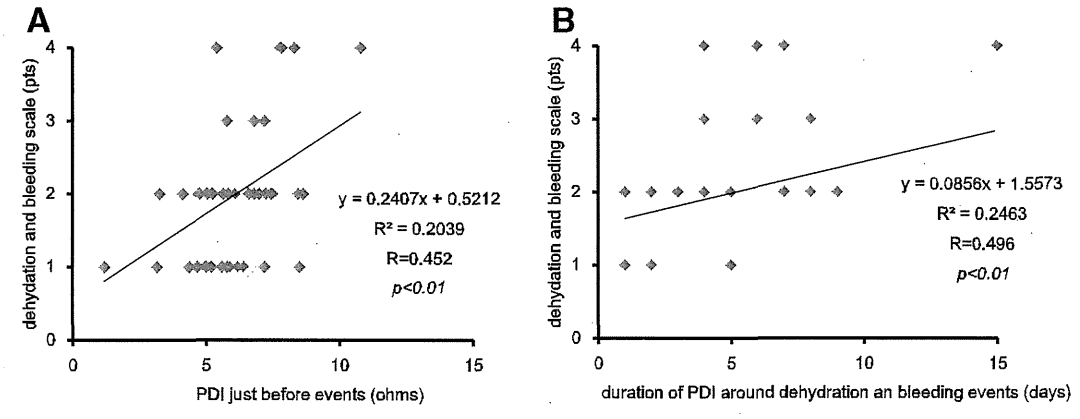

Figure 5. Correlation between positive deviation of thoracic impedance (PDI) size and the severity of the dehydration and bleeding events. A dot plot of the newly developed dehydration and bleeding scale scores in relation to the peak level of each PDI just before (day 1), the dehydration and bleeding events (**A**), and through the duration of each PDI (**B**). The clinical severity of dehydration and bleeding correlated significantly with the peak level and duration of the PDI.

followed by a large PDI pattern. This pattern reflected congestion and dehydration due to the over use of diuretics (Figures 3A,B). Interestingly, a significant elevation of blood urea nitrogen (BUN)/serum creatinine (Cr) ratio and significant symptoms of dehydration were observed during periods of large PDI (Figure 3C). Moreover, impedance increased 3 days prior to symptoms of dehydration and BUN/Cr ratio elevation. These results might indicate that the increase in the thoracic impedance prior to clinical symptoms and/or blood chemistry data might indicate dehydration.

Volume Loss Case 2: Bleeding Case

Figure 4 summarizes a case of a patient with chronic heart failure due to ischemic cardiomyopathy. He had atrial fibrillation and had taken oral anti-coagulants along with dual antiplatelet agents for drug-eluting stent implantation. Anemia from gastrointestinal bleeding due to gastric ulceration disrupted his hemodynamics. A blood transfusion was performed after the administration of saline because of low output syndrome due to rapid bleeding. A large PDI in thoracic impedance was recorded, as shown in Figures 4A and B. An acute increase of thoracic impedance from baseline and a relatively slow recovery was consistent with the rapid clinical course of volume loss and its recovery. In fact, the hemoglobin level was decreased from 110 g/L to 79 g/L and recovered to baseline after a blood transfusion (Figure 4B). These results indicated that a large PDI was consistent with the period of volume loss events due to bleeding.

Peak Level and Duration of PDI Correlated With the Severity of Volume Loss Events

Among 86 PDIs with volume loss events, the correlation between the clinical severity of the volume loss event and the morphology of the PDI was analyzed. Dehydration and bleeding scale scores reflecting the clinical severity of the volume loss events were defined based on the type of treatment provided, such education, adjustment of medications, admission, catecholamine administration for low output and blood infusions for recovery. The peak levels and durations of PDI were found to be correlated with the clinical severity of the volume loss event (Figures 5A,B). These results indicate that the height of the PDI might predict the severity and clinical course of the volume loss event.

Discussion

Pulmonary congestion including vascular congestion and interstitial congestion would decrease intrathoracic impedance.[9,10] The continuous monitoring of intrathoracic impedance has been used in the detection of acute decompensated heart failure.[11] OptiVol fluid status monitoring is the application of intrathoracic impedance for the measurement of pulmonary fluid retention.[11] In contrast, thoracic impedance is considered to increase along with fluid loss during optimal heart failure treatment using intense diuretics.[10] Moreover, the feasibility of the concept of detecting volume loss as an increase in thoracic impedance was illustrated in an animal model.[8] However, the clinical feasibility of increased intrathoracic impedance detection of volume loss events is not known.

This study defined several categories of positive deviation of intrathoracic impedance from the reference line (PDI) including no PDI, small PDI, spike PDI and large PDI (Figures 1A–D). In addition, the association between these PDIs and clinical volume loss events like dehydration and bleeding were investigated in chronic heart failure patients (NYHA II, III or IV; Table 1). A large PDI showed a high PPV (100%) for the detection of volume loss events, but this was not the case for a small PDI (22.1%) and a spike PDI (51.7%). A clinical trial investigating whether intrathoracic impedance monitoring (OptiVol) with audible patient alerts could improve the outcome of heart failure patients failed to show its clinical utility.[12] In addition, the number of hospitalizations significantly increased in the OptiVol patient alert guiding therapy group in comparison to the conventional groups.[12] The concept of identifying a decrease in thoracic impedance for the early detection of decompensated heart failure before hospitalization had been reported by many groups.[10,13–18] However, the PPV of the OptiVol patient alert is 38.1% at the nominal Fluid Index threshold.[18] It is impossible to disregard the pseudo-positive signal from a patient alert. The main cause of unnecessary hospitalization in the OptiVol patient alert group might be due to the low PPV of the Fluid index.[12] Therefore, the current study defined several PDI categories and analyzed which PDI showed a high PPV for the early detection of volume loss events. Although the sensitivity of a large PDI (32.1%) is by no means satisfactory, the high PPV is thought to be the most attractive indicator for the early detection of an impending volume loss event before hospitalization and for decreasing unnecessary hospitalization due to alerts from impedance monitoring.

The variability of thoracic impedance during decompensated congestive heart failure treatment followed by dehydration due to an over-dose use of diuretics showed a large PDI after a dip in the impedance under the reference line in some cases like case 1 (Figure 3). In contrast, dehydration without prior decompensated heart failure or bleeding events showed an acute up slope from the reference line without any decrease in impedance before a large PDI, as in case 2 (Figure 4). These different patterns around a large PDI formation might help to identify the clinical features before hospitalization.

Moreover, a correlation between the peak level of PDI and the severity of the volume loss event was observed (Figure 5A). Awareness of this relationship might therefore be useful when choosing a suitable strategy for treating each volume loss event.

In this study, we selected heart failure patients (NYHA II, III or IV) and excluded patients who had implanted devices within 1 year to completely avoid the impact of postsurgical edema and inflammation in the pocket area.[11] Although, the number of enrolled patients was low, it was possible to record sufficient volume loss events and PDIs without any surgical or infectious noise.

Study Limitations

The limitations of this study include that it was a single-center retrospective study with no of long-term follow up. Larger and prospective studies are needed to further assess the clinical feasibility of continuous intrathoracic impedance monitoring to predict volume loss events in chronic heart failure patients.

Conclusions

The present study is the first demonstration of the association of continuous intrathoracic impedance monitoring by implanted devices (CRTD and ICD) and volume loss events in chronic heart failure patients. A large PDI was useful and new criteria to catch the volume loss events with high PPV in severe chronic heart failure patients after they are implanted with devices with continuous thoracic impedance monitoring was established. Continuous intrathoracic impedance monitoring might be used for the prediction of volume loss events with high PPV by using well-defined criteria.

Acknowledgments

We gratefully acknowledge Takahide Murasawa, Susumu Miyazaki, Jun Yokota, Keigo Iwazaki for their excellent technical assistance. This research is supported by the Japan Society for the Promotion of Science (JSPS) through its "Funding Program for World-Leading Innovative R&D on Science and Technology (FIRST Program)".

References

1. Seo Y, Ito H, Nakatani S, Takami M, Naito S, Shiga T, et al. The role of echocardiography in predicting responders to cardiac resynchronization therapy: Results from the Japan cardiac resynchronization therapy registry trial (J-CRT). *Circ J* 2011; **75:** 1156–1163.
2. Dickstein K, Cohen-Solal A, Filippatos G, McMurray JJ, Ponikowski P, Poole-Wilson PA, et al. ESC guidelines for the diagnosis and treatment of acute and chronic heart failure 2008: The Task Force for the Diagnosis and Treatment of Acute and Chronic Heart Failure 2008 of the European Society of Cardiology. Developed in collaboration with the Heart Failure Association of the ESC (HFA) and endorsed by the European Society of Intensive Care Medicine (ESICM). *Eur J Heart Fail* 2008; **10:** 933–989.
3. Kinugawa K. How to treat stage d heart failure?: When to implant left ventricular assist devices in the era of continuous flow pumps? *Circ J* 2011; **75:** 2038–2045.
4. Tsutsui H, Tsuchihashi M, Takeshita A. Mortality and readmission of hospitalized patients with congestive heart failure and preserved versus depressed systolic function. *Am J Cardiol* 2001; **88:** 530–533.
5. Kato N, Kinugawa K, Seki S, Shiga T, Hatano M, Yao A, et al. Quality of life as an independent predictor for cardiac events and death in patients with heart failure. *Circ J* 2011; **75:** 1661–1669.
6. Cleland JGF, Swedberg K, Follath F, Komajda M, Cohen-Solal A, Aguilar JC, et al; Study Group on Diagnosis of the Working Group on Heart Failure of the European Society of Cardiology. The Euro-Heart Failure survey programme–a survey on the quality of care among patients with heart failure in Europe. Part 1: Patient characteristics and diagnosis. *Eur Heart J* 2003; **24:** 442–463.
7. McMurray JJV, Teerlink JR, Cotter G, Bourge RC, Cleland JGF, Jondeau G, et al. Effects of tezosentan on symptoms and clinical outcomes in patients with acute heart failure. *JAMA* 2007; **298:** 2009–2019.
8. Krantz T, Cai Y, Lauritsen T, Warberg J, Secher NH. Accurate monitoring of blood loss: Thoracic electrical impedance during hemorrhage in the pig. *Acta Anaesthesiol Scand* 2000; **44:** 598–604.
9. Wang LI, Lahtinen S, Lentz L, Rakow N, Kaszas C, Ruetz L, et al. Feasibility of using an implantable system to measure thoracic congestion in an ambulatory chronic heart failure canine model. *Pacing Clin Electrophysiol* 2005; **28:** 404–411.
10. Yu CM, Wang L, Chau E, Chan RHW, Kong SL, Tang MO, et al. Intrathoracic impedance monitoring in patients with heart failure. *Circulation* 2005; **112:** 841–848.
11. Li W. Fundamentals of intrathoracic impedance monitoring in heart failure. *Am J Cardiol* 2007; **99:** S3–S10.
12. van Veldhuisen DJ, Braunschweig F, Conraads V, Ford I, Cowie MR, Jondeau G, et al. Intrathoracic impedance monitoring, audible patient alerts, and outcome in patients with heart failure/clinical perspective. *Circulation* 2011; **124:** 1719–1726.
13. Vollmann D, Nägele H, Schauerte P, Wiegand U, Butter C, Zanotto G, et al. Clinical utility of intrathoracic impedance monitoring to alert patients with an implanted device of deteriorating chronic heart failure. *Eur Heart J* 2007; **28:** 1835–1840.
14. Ypenburg C, Bax JJ, van der Wall EE, Schalij MJ, van Erven L. Intrathoracic impedance monitoring to predict decompensated heart failure. *Am J Cardiol* 2007; **99:** 554–557.
15. Maines M, Catanzariti D, Cemin C, Vaccarini C, Vergara G. Usefulness of intrathoracic fluids accumulation monitoring with an implantable biventricular defibrillator in reducing hospitalizations in patients with heart failure: A case-control study. *J Interv Card Electrophysiol* 2007; **19:** 201–207.
16. Whellan DJ, Ousdigian KT, Al-Khatib SM, Pu W, Sarkar S, Porter CB, et al. Combined heart failure device diagnostics identify patients at higher risk of subsequent heart failure hospitalizations: Results from PARTNERS HF (program to access and review trending information and evaluate correlation to symptoms in patients with heart failure) study. *J Am Coll Cardiol* 2010; **55:** 1803–1810.
17. Packer M, Abraham WT, Mehra MR, Yancy CW, Lawless CE, Mitchell JE, et al. Utility of impedance cardiography for the identification of short-term risk of clinical decompensation in stable patients with chronic heart failure. *J Am Coll Cardiol* 2006; **47:** 2245–2252.
18. Conraads VM, Tavazzi L, Santini M, Oliva F, Gerritse B, Yu CM, et al. Sensitivity and positive predictive value of implantable intrathoracic impedance monitoring as a predictor of heart failure hospitalizations: The SENSE-HF trial. *Eur Heart J* 2011; **32:** 2266–2273.

Cell Stem Cell
Resource

Distinct Metabolic Flow Enables Large-Scale Purification of Mouse and Human Pluripotent Stem Cell-Derived Cardiomyocytes

Shugo Tohyama,[1,3] Fumiyuki Hattori,[1,4,*] Motoaki Sano,[1] Takako Hishiki,[2] Yoshiko Nagahata,[2,5] Tomomi Matsuura,[2,5] Hisayuki Hashimoto,[1] Tomoyuki Suzuki,[6] Hiromi Yamashita,[1,4] Yusuke Satoh,[1] Toru Egashira,[1] Tomohisa Seki,[1] Naoto Muraoka,[1] Hiroyuki Yamakawa,[1] Yasuyuki Ohgino,[1] Tomofumi Tanaka,[4] Masatoshi Yoichi,[4] Shinsuke Yuasa,[1] Mitsushige Murata,[1] Makoto Suematsu,[2,5] and Keiichi Fukuda[1,*]
[1]Department of Cardiology
[2]Department of Biochemistry
Keio University School of Medicine, Tokyo 160-8582, Japan
[3]Japan Society for the Promotion of Science, Tokyo 102-8472, Japan
[4]Asubio Pharma, Kobe 650-0047, Japan
[5]Japan Science and Technology Agency (JST), Exploratory Research for Advanced Technology (ERATO) Suematsu Gas Biology Project, Tokyo 160-8582, Japan
[6]Department of Cardiovascular Research, Research Institute of Environmental Medicine, Nagoya University, Nagoya 464-8601, Japan
*Correspondence: hattori.fumiyuki.ef@asubio.co.jp (F.H.), kfukuda@a2.keio.jp (K.F.)
http://dx.doi.org/10.1016/j.stem.2012.09.013

SUMMARY

Heart disease remains a major cause of death despite advances in medical technology. Heart-regenerative therapy that uses pluripotent stem cells (PSCs) is a potentially promising strategy for patients with heart disease, but the inability to generate highly purified cardiomyocytes in sufficient quantities has been a barrier to realizing this potential. Here, we report a nongenetic method for mass-producing cardiomyocytes from mouse and human PSC derivatives that is based on the marked biochemical differences in glucose and lactate metabolism between cardiomyocytes and noncardiomyocytes, including undifferentiated cells. We cultured PSC derivatives with glucose-depleted culture medium containing abundant lactate and found that only cardiomyocytes survived. Using this approach, we obtained cardiomyocytes of up to 99% purity that did not form tumors after transplantation. We believe that our technological method broadens the range of potential applications for purified PSC-derived cardiomyocytes and could facilitate progress toward PSC-based cardiac regenerative therapy.

INTRODUCTION

Heart disease is a common and deadly disease, and heart-regenerative therapy is a promising therapeutic strategy for some patients (Passier et al., 2008). Pluripotent stem cells (PSCs) including embryonic stem cells (ESCs) and induced pluripotent stem cells (iPSCs) are potential sources for production of therapeutic cardiomyocytes (Burridge et al., 2012; Takahashi et al., 2007; Thomson et al., 1998). A typical human left ventricle contains roughly 6×10^9 cardiomyocytes; thus, nearly 1×10^9 de novo cardiomyocytes would be required per patient for this type of repair (Hattori and Fukuda, 2012). However, PSC-based approaches carry a high risk of tumor formation due to contamination of residual PSCs in the therapeutic cell preparations. Therefore, obtaining highly purified cardiomyocytes will be key for achieving therapeutic success in applying these cells.

Procedures involving density-gradient centrifugation (Laflamme et al., 2007; Xu et al., 2006), genetic modification (Fijnvandraat et al., 2003; Gassanov et al., 2004; Hidaka et al., 2003; Klug et al., 1996), and nongenetic methods that use a mitochondrial dye (Hattori et al., 2010) or antibodies to specific cell-surface markers (Dubois et al., 2011; Uosaki et al., 2011) have been established for cardiomyocyte enrichment. However, none of these methods are ideal for the therapeutic application of PSC-derived cardiomyocytes because of drawbacks including insufficient purity, genotoxicity, and the use of fluorescence-activated cell sorting (FACS) and/or antibodies.

Glucose is the main source of energy and anabolic precursors in various mammalian cells. It is converted by glycolysis into pyruvate and/or lactate via glucose-6-phosphate (G6P; a source of nucleotides) and 3-phosphoglycerate (a source of some amino acids) for generation of two ATP molecules without the need for oxygen. Pyruvate is further utilized in the mitochondrial tricarboxylic acid (TCA) cycle for production of 36 ATP molecules via oxidative phosphorylation (OXPHOS). Cardiomyocytes efficiently produce energy from several substrates including glucose, fatty acids, and lactate via OXPHOS. Interestingly, there are marked changes between energy substrate utilization by cardiomyocytes before and after birth. The fetal heart has a higher capacity for lactate uptake than the adult heart (Fisher et al., 1981) and uses lactate as a major energy source (Neely and Morgan, 1974; Werner and Sicard, 1987) by exploiting the lactate-rich environment created by the placenta (Burd et al., 1975).

In this study, we took advantage of the unique metabolic properties of cardiomyocytes to develop an efficient and

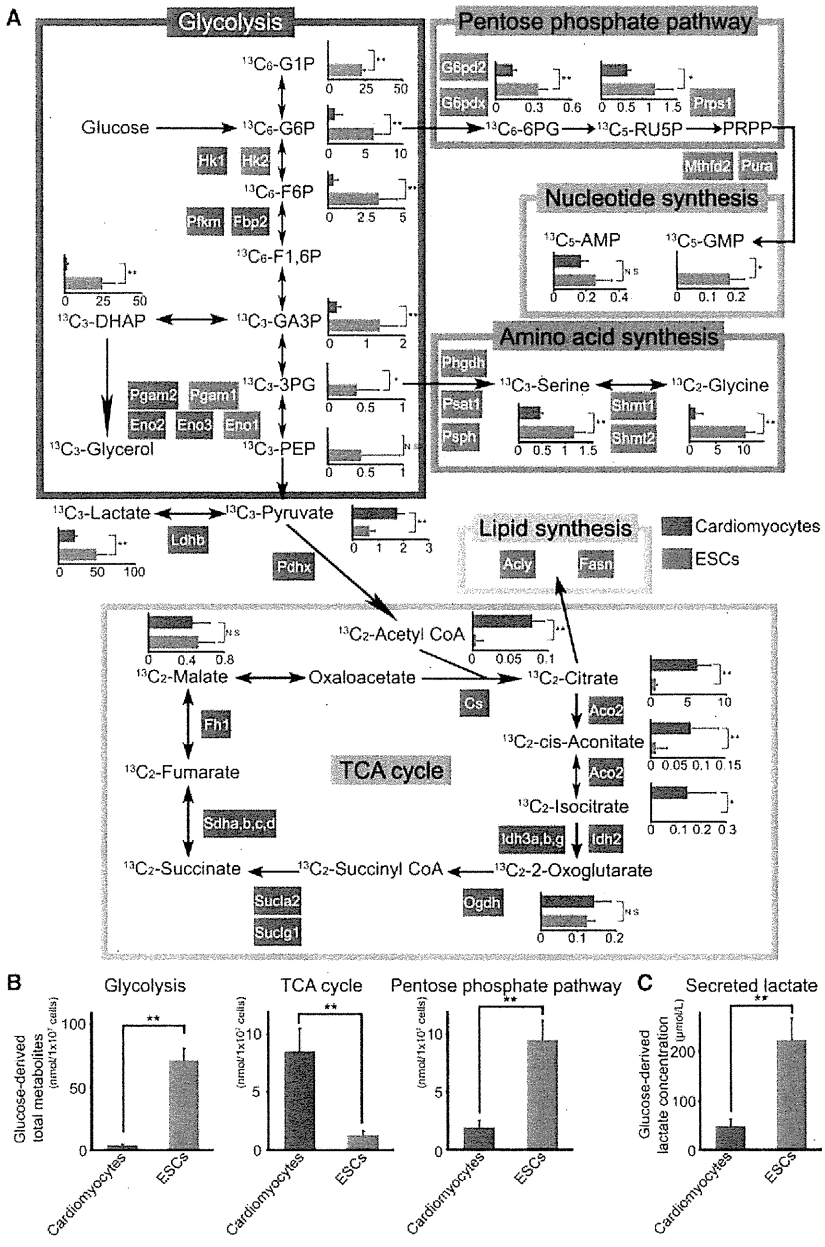

Figure 1. Distinct Metabolic Differences Between Cardiomyocytes and ESCs in Transcriptome and Fluxome Analyses

(A) Metabolic pathway map summarizing the results from gene array and [^{13}C]-labeled glucose fluxome analyses. Gene names shown in red or blue boxes indicate the mRNA expression levels increased more than 2-fold in cardiomyocytes or ESCs, respectively. The bar graphs represent the detected levels of [^{13}C]-labeled metabolites in cardiomyocytes (red bar) and ESCs (blue bar) (n = 4). All units are nmol per 1.0 × 10^7 cells. All data were obtained from independent experiments.

(B) Total [^{13}C]-labeled metabolites of cardiomyocytes (red bar) and ESCs (blue bar) in each key pathway (n = 4).

(C) Secreted [^{13}C]-labeled lactate concentration in the media of cardiomyocytes (red bar) and ESCs (blue bar) (n = 4). All data were obtained from independent experiments.

*$p < 0.05$; **$p < 0.01$. Data are shown as mean ± SD. All the abbreviations are shown in Table S1. See also Figure S1 and Table S1.

noninvasive environmental approach for their purification from PSC cultures.

RESULTS

Integrated Transcriptomic and Metabolomic Analyses Highlight Distinct Metabolic Differences between Cardiomyocytes and Other Proliferating Cells

To find metabolism-related genes that are differentially expressed between undifferentiated stem cells and cardiomyocytes, we performed comparative transcriptome analyses of undifferentiated mouse ESCs and neonatal mouse cardiomyocytes purified by the "mitochondrial method"(Hattori et al., 2010) (Figures S1A and S1B available online). The results for cardiomyocytes revealed markedly higher expression of genes encoding enzymes involved in the TCA cycle than the undifferentiated ESCs and, in turn, lower expression of genes involved in the pentose phosphate, amino acid synthesis, and lipid synthesis pathways (Figure 1A and Table S1). Next, we conducted a fluxome analysis (Kinoshita et al., 2007; Shintani et al., 2009) to trace a range of metabolites derived from [^{13}C]-labeled glucose in neonatal rat cardiomyocytes, mouse ESCs, a hepatocyte cell line (HepG2), and a skeletal myoblast cell line (C2C12). [^{13}C]-labeled intermediate metabolites of the glycolytic, pentose phosphate, and amino acid synthesis pathways were subsequently found at higher levels in ESCs, HepG2, and C2C12 cells than in cardiomyocytes (Figures 1A, 1B, and S1C and Table S1). ESCs, HepG2, and C2C12 cells also discarded more lactate than cardiomyocytes did (Figure 1C and Figure S1D). In contrast, cardiomyocytes took up pyruvate into mitochondria, and most [^{13}C]-labeled intermediate metabolites of the TCA cycle were significantly higher in cardiomyocytes than in ESCs (Figure 1A). These transcriptome and fluxome analyses highlighted a dynamic difference in the metabolic fates of lactate between cell types (Figure S1E). More specifically, lactate was discarded by noncardiomyocytes but preferentially used in TCA metabolism by cardiomyocytes. We hypothesized that cells mainly dependent on glycolysis might not be able to survive under glucose-depleted and lactate-abundant conditions, whereas cardiomyocytes would survive by using lactate as an alternative energy source.

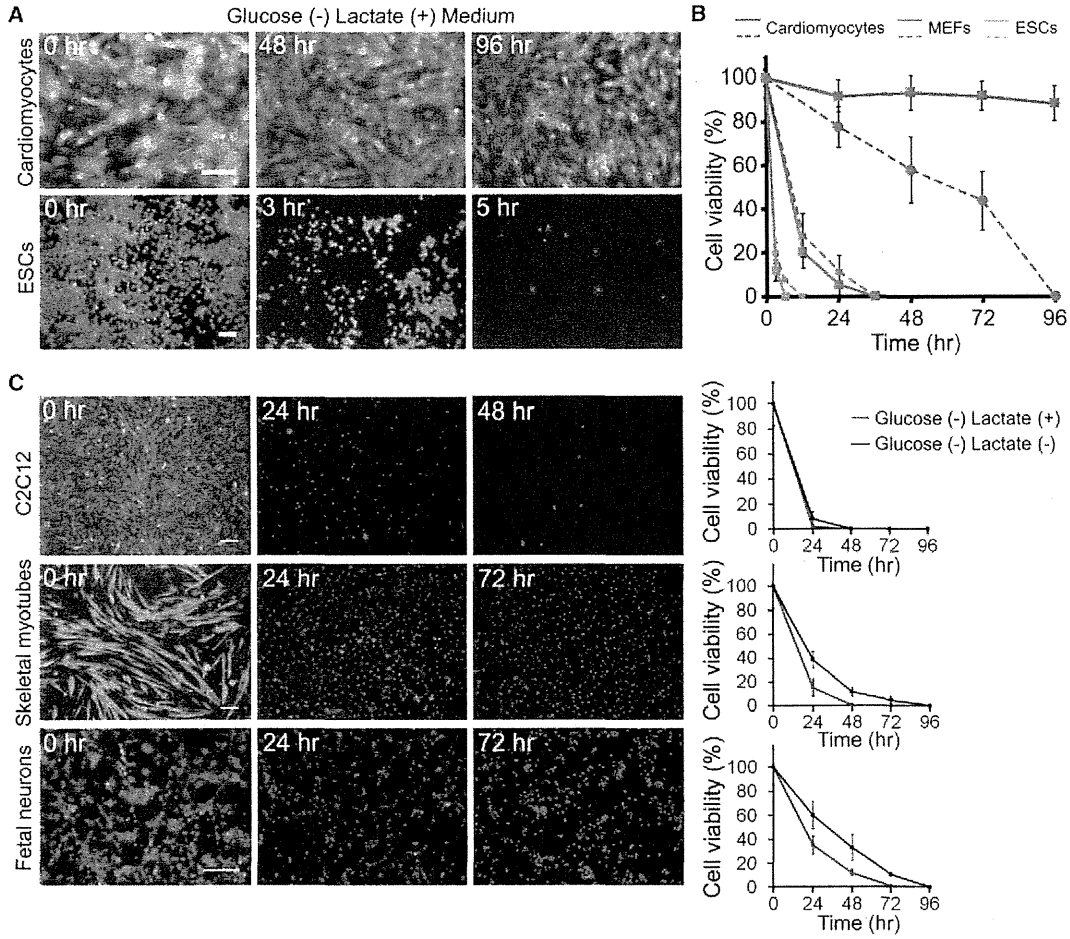

Figure 2. Cell Viabilities of Various Cells under Glucose-Depleted and Lactate-Supplemented Conditions

(A) Cultured neonatal rat cardiomyocytes and mouse ESCs were exposed to glucose-depleted media supplemented with lactate, and their viabilities were assessed with the LIVE/DEAD kit, which indicates viable cells with green fluorescence and dead cells with nuclear red fluorescence.

(B) Time course of viability in neonatal rat cardiomyocytes (red), mouse ESCs (blue), and MEFs (green) under glucose-free conditions with and without lactate (n = 6). Solid lines indicate the glucose-free and lactate-supplemented condition, and dashed lines indicate the glucose-free without lactate condition. All data were obtained from independent experiments.

(C) Noncardiomyocytes including C2C12, skeletal myotubes, and primary cultured neurons were exposed to glucose-free conditions with and without lactate, and their viabilities were assessed with the LIVE/DEAD kit. The time courses of viability were plotted in the line graphs (right) (all cells; n = 4). Red lines indicate the glucose-free and lactate-supplemented condition, and black lines indicate the glucose-free without lactate condition. The inset in primary neurons represents immunocytochemical staining with an antibody to βIII-tubulin (red) and with DAPI (blue).

Scale bars represent 100 μm (A and C). Data are shown as mean ± SD. See also Figure S2.

Glucose-Depleted and Lactate-Enriched Culture Conditions Can Purify Cardiomyocytes from Mouse and Human PSC Derivatives

To test our hypothesis, we exposed neonatal rat cardiomyocytes, mouse ESCs, primary peripheral lymphatic cells, primary fetal neurons, primary mouse embryonic fibroblasts (MEFs), C2C12 cells (myoblasts and myotubes), hepatocytes (HepG2), and renal cells (HEK293) to glucose-depleted conditions with and without various concentrations of lactate. Every type of cell died within 96 hr in the glucose-depleted conditions, and as expected, supplementation with lactate only prolonged the survival of cardiomyocytes (Figures 2A, 2B, 2C and S2). We named this special culture condition for the growth of cardiomyocytes the "lactate method."

We next applied the lactate method to purifying human PSC-derived cardiomyocytes. First, we optimized the time course of the method for human ESC (hESC)-derived cardiomyocytes. Using time-lapse imaging, we observed that 7 days' exposure of hESC- and human iPSC (hiPSC)-derived attached embryoid bodies (EBs) to glucose-free conditions supplemented with 4 mM lactate selectively enriched for beating cells (Movie S1). Second, we confirmed that days 7–8 of culture were the best time points for harvesting the cells, as shown in Figure 3A. To optimize the lactate concentration, we measured the viability

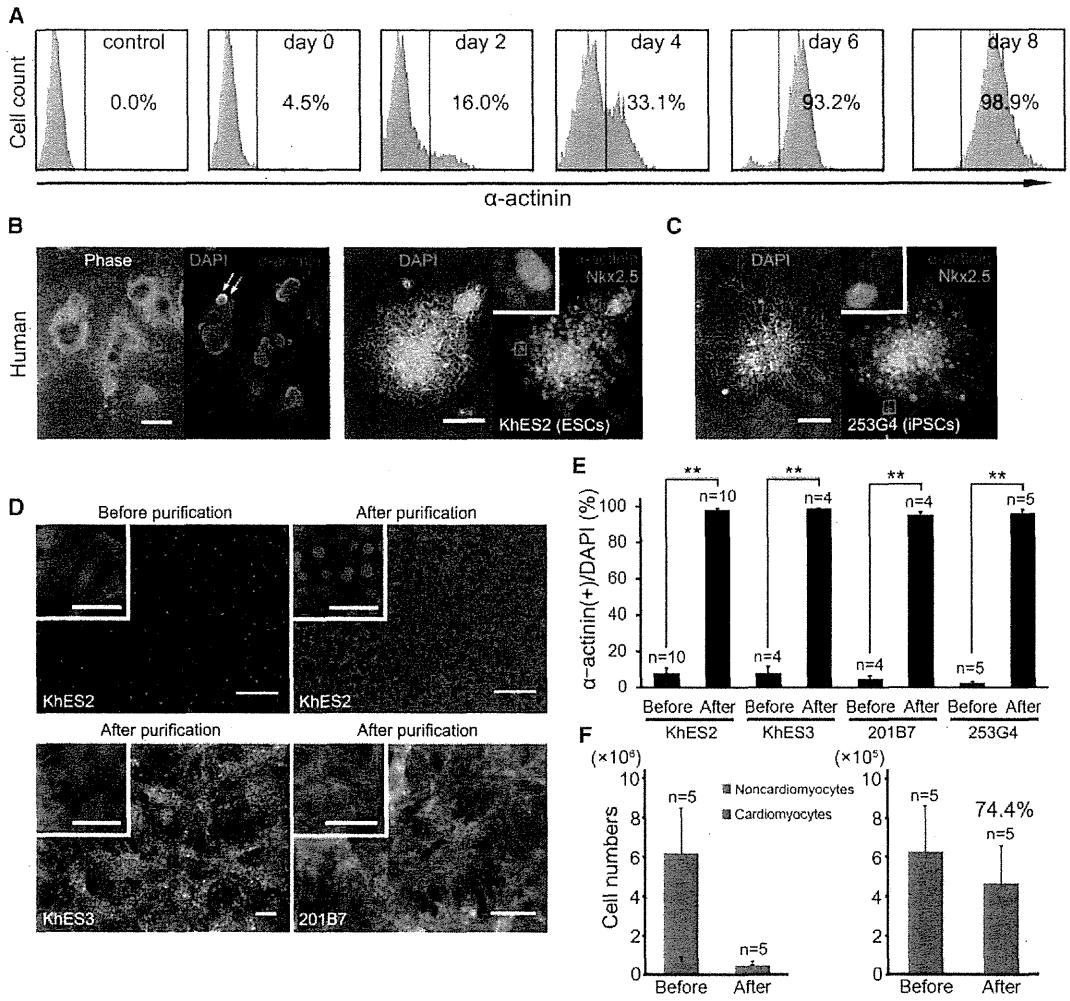

Figure 3. Purification of Cardiomyocytes under Glucose-Depleted and Lactate-Supplemented Conditions

(A) Representative FACS analyses for α-actinin expression in the hESC-derived cells during metabolic selection. Control indicates hESC-derived cells after 2 days of differentiation that do not contain any cardiomyocytes.

(B and C) Representative phase-contrast and immunofluorescent staining for α-actinin in the nonpurified hESC-derived EBs (B, left) and for α-actinin and Nkx2.5 in purified hESC (KhES-2)-derived cardiomyocytes (hESC-CMs) (B, right) and purified hiPSC (253G4)-derived cardiomyocytes (hiPSC-CMs) (C). Arrows indicate α-actinin-positive cells.

(D) Representative immunofluorescent staining for α-actinin (red) in the hESC (KhES-2 and KhES-3)- and hiPSC (201B7)-derived dispersed cells before (upper left) and after (upper right, lower panels) metabolic selection. The cell nuclei are stained by DAPI (blue).

(E) Percentage of α-actinin-positive cardiomyocytes in the hESC (KhES-2 and KhES-3)- and hiPSC (201B7 and 253G4)-derived dispersed cells before and after metabolic selection. All data were obtained from independent experiments.

(F) Numbers of α-actinin-negative noncardiomyocytes (green) and α-actinin-positive cardiomyocytes (red) in the hESC-derived dispersed cells before (n = 5) and after (n = 5) metabolic selection (left graph). The right graph represents only α-actinin-positive cardiomyocytes. All data were obtained from independent experiments.

Scale bars represent 50 μm (D, insets), 100 μm (B, right; C and D, lower panels), and 500 μm (B, left; D, upper panels). **p < 0.01. Data are shown as mean ± SD. See also Figure S3 and Movies S1, S2, and S3.

of purified hESC-derived cardiomyocytes exposed to glucose-depleted conditions with various concentrations of lactate for 6 days; we found the lowest numbers of dead cells in 4 mM lactate (Figure S3A). We further tested for the ideal period of differentiation using the lactate method and found that 20–30 days of differentiation produced the highest reproducibility, purity, and yield of cardiomyocytes. To determine why this period is optimal, we investigated the proliferative activity of EBs on various differentiation days (days 14–60) using a 5-ethynyl-20-deoxyuridine (EdU) incorporation assay. The percentage of EdU-incorporated cells markedly decreased after day 30 (Figure S3B), implying that proliferating cells are sensitive to the lactate method. The optimized condition efficiently enriched for globally contracting aggregates in a time-dependent manner (Figure S3C and Movie S2). Concomitantly, messenger RNA (mRNA) expression of the cardiomyocyte-related gene

MYH6 increased, while that of the pluripotency-related gene *POU5F1* (Figure S3D) decreased abruptly. In addition, the mRNAs for noncardiac genes (*NANOG*, *MYOD*, *AFP*, and *MAP2*) were completely eliminated, and those for other cardiomyocyte-related genes (*ACTC1* and *NKX2.5*) were significantly enriched (Figures S3E and S3F). We also observed clumps of purified cardiomyocytes in the adhered condition (Figures 3B and 3C). We dispersed the clumps and cultured the cells therein and then evaluated their purity before and after metabolic selection. The percentages of α-actinin-positive cells before and after metabolic selection were 8.1 ± 2.9% (n = 10) and 98.3 ± 0.9% (n = 10), respectively (Figures 3D and 3E). We also confirmed the efficacy of the lactate method using other hESC (KhES-3) and hiPSC (201B7 and 253G4) lines. As shown in Figures 3D and 3E, the purities were determined as 98.9 ± 0.3, 95.5 ± 1.3, and 96.5 ± 2.0%, respectively. To identify selective events in KhES-2 and iPSCs (253G4 and 201B7), we obtained global gene-expression patterns for the PSC-derived EBs and purified hESC-derived cardiomyocytes. We categorized the expressed genes following the gene ontology consortium and found both similarities and differences among EBs derived from three cell lines (Ashburner et al., 2000). One possible explanation for the differences is that the derived EBs contain various types of cells that are eventually eliminated by the lactate-purification method (Figures S3G and S3H). In our system, 4.0×10^6 hESCs differentiated into $6.2 \pm 2.5 \times 10^6$ (n = 5) cells containing $6.3 \pm 2.3 \times 10^5$ (n = 5) α-actinin-positive cardiomyocytes, and $4.7 \pm 1.8 \times 10^5$ (n = 5) α-actinin-positive cardiomyocytes were finally purified via the lactate method. Therefore, the yield-based efficiency of our lactate method for hESCs was 74.4 ± 12.1% (Figure 3F). To directly compare the yield-based efficiencies between the lactate method and our previous mitochondrial method, we evaluated the yield and found 52.9 ± 12.8% recovery of cardiomyocytes in our previous mitochondrial method (Figure S3I). To determine the types of noncardiomyocyte cells remaining after metabolic selection, we performed immunocytochemical screening and found that most of the cells were smooth muscle actin (SMA)-positive (Figure S3J). Interestingly, α-actinin- and SMA-double-positive cells were also found (data not shown), consistent with a previous report that immature cardiomyocytes express SMA (Clément et al., 2007).

We then applied the lactate method to mouse ESCs using lactate concentrations and timings optimized through similar preliminary experiments for mouse cells. EBs attached to the dishes were exposed to glucose-depleted and 1 mM lactate-supplemented conditions. After 7 days of selection, we recovered the surviving cells by collagenase digestion and transferred them into new fibronectin-coated plates (Movie S3). Immunofluorescence staining revealed that most of the surviving cells were positive for the cardiac markers α-actinin and GATA4 (99.4 ± 0.6% purity, n = 5) (Figure S3K).

Cardiomyocytes Showed High Lactate Uptake and Used Lactate for Metabolic-Energy Production

Why do only cardiomyocytes survive under the lactate-method condition? To address this question, we first compared the [^{14}C]-lactate uptake activity of neonatal rat and human ESC-derived cardiomyocytes, ESCs, MEFs, and noncontracting EBs, and found that both cardiomyocyte populations showed higher levels of activity than the other cells (Figures 4A and 4C). We then measured the changes in intracellular ATP levels in cardiomyocytes and other cells under lactate-method conditions and found that the levels in mouse ESCs, MEFs, and noncontracting EBs fell abruptly, whereas those in neonatal rat and purified human ESC-derived cardiomyocytes were sustained for significantly longer (Figures 4B and 4D). These results indicated that cardiomyocytes, but not noncardiomyocytes, can effectively uptake and use lactate to maintain ATP levels.

Lactate supplementation has the potential to cause acidification either intracellularly or in the medium, which could lead to cellular damage. We therefore investigated whether 4 mM lactate supplementation affects extra- and intracellular pH values. The extracellular pH values were stable at 7.5 following 1 hr of incubation in a 5% CO_2 incubator (Figure S4A). The intracellular pH values of cardiomyocytes, mouse ESCs, MEFs, and C2C12 myoblasts were not affected by supplementation with 4 mM lactate, but all were significantly decreased by the addition of 20 mM lactate (Figures S4B and S4C). Lactate can be transported by monocarboxylic acid transporters (MCTs), of which subtype 1 is abundantly expressed in muscle cells and localizes at both the plasma and mitochondrial inner membrane (Hashimoto et al., 2006). For investigation of the significance of MCT1 expression for lactate uptake in cardiomyocytes, the cells were treated with MCT1 inhibitor α-cyano-4-hydroxycinnamate (α-CHC) (Sonveaux et al., 2008) under glucose-free and lactate-rich conditions. The lactate-induced prolonged survival of cardiomyocytes under glucose-free conditions was largely abolished by the MCT1 inhibitor, despite the lack of α-CHC toxicity, suggesting that lactate uptake via MCT1 plays a major role in the long-term survival of cardiomyocytes under metabolic selection (Figure 4E). To investigate why cardiomyocytes can effectively take up lactate, we checked the expression levels of MCT1 in cardiomyocytes and ESCs but could not find a marked difference between the two (Table S1). We then performed electron microscopy on the hESCs and their derivative cardiomyocytes, as well as mitochondrial staining of hESC-derived cells. The cardiomyocytes showed substantially higher numbers of mitochondria than ESCs and other noncardiomyocytes (Figures S4D and S4E). Because MCTs are passive transporters, we suggest that a major mechanism underlying the enhanced lactate uptake in cardiomyocytes could be the concentration gradients generated by effective lactate consumption via the highly active TCA cycle.

We further investigated how lactate is metabolized in various types of cells. We performed lactate fluxome analysis in mouse ESCs, hESC-derived EBs, MEFs, and neonatal rat cardiomyocytes under glucose-depleted conditions for short (30 min) periods. As expected, high levels of [2,4,5-^{13}C]-citrate, [3,4-^{13}C]-succinate, and [2,3,4-^{13}C]-malate were detected in cardiomyocytes, whereas the ESCs, hESC-derived EBs, and MEFs showed only small amounts of these metabolites, suggesting that exogenous lactate is more efficiently metabolized via the TCA cycle in cardiomyocytes than in noncardiomyocytes, including ESCs (Figure 5 and Figure S5). To our surprise, [^{13}C]-labeled glycolytic intermediates including G6P were observed in both cardiomyocytes and ESCs. These were eventually consumed in the pentose phosphate pathway for production of inosine, guanosine, and adenosine monophosphates.

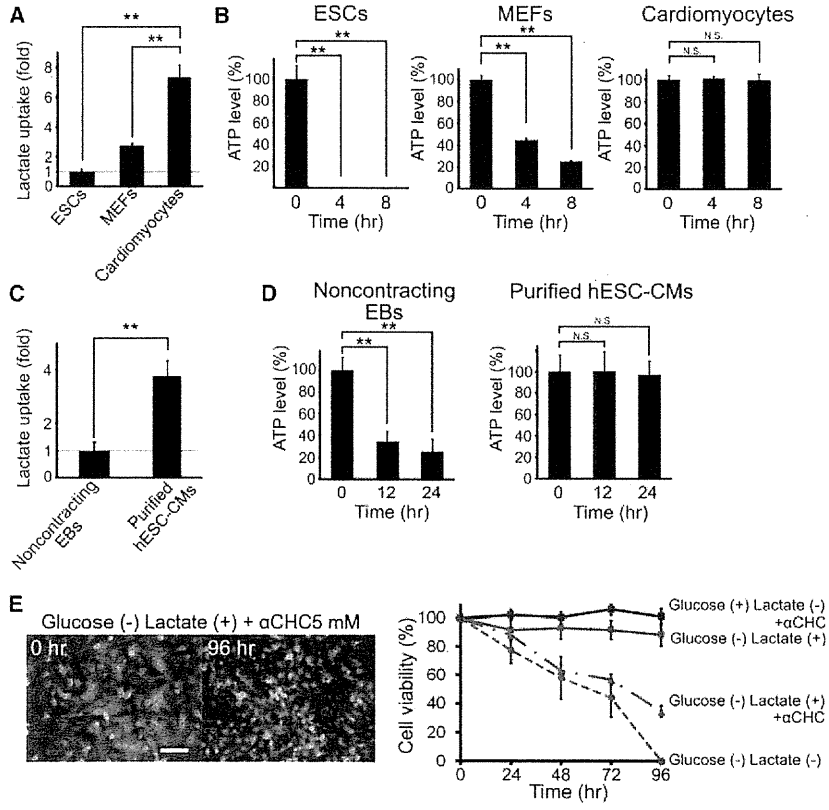

Figure 4. Lactate Uptake and Energetic Homeostasis in Various Types of Cells under Glucose-Depleted and Lactate-Supplemented Conditions

(A and C) [^{14}C]-labeled lactate uptake abilities in (A) mouse ESCs, MEFs, and rat neonatal cardiomyocytes (n = 3) and (C) in noncontracting hESC-derived EBs and purified hESC-CMs (n = 3). All data were obtained from independent experiments.

(B and D) Intracellular ATP levels in (B) the mouse ESCs, MEFs, and neonatal cardiomyocytes (n = 3), and (D) in noncontracting hESC-derived EBs and purified hESC-CMs (n = 3) under glucose-depleted and lactate-supplemented conditions. Relative ATP levels are indicated as percentages of the levels in untreated samples. All data were obtained from independent experiments.

(E) Cultured neonatal rat cardiomyocytes were exposed to glucose-free with lactate conditions supplemented with MCT1 inhibitor (α-CHC, 5 mM), and their viabilities were visualized using the LIVE/DEAD kit (left). The time course of the cardiomyocyte viabilities under different culture conditions is shown (right). Chain and solid red lines indicate glucose-depleted and lactate-supplemented medium supplemented with (n = 4) and without (n = 6) MCT1 inhibitor, respectively. The dashed red line indicates the glucose-depleted without lactate condition (n = 6). The blue solid line indicates high-glucose medium supplemented with MCT1 inhibitor (n = 4). All data were obtained from independent experiments.

Scale bar represents 100 μm (E). *$p < 0.05$; **$p < 0.01$. Data are shown as mean ± SD. See also Figure S4.

Long-period (24 hr) fluxome analysis in viable cardiomyocytes also detected [5-^{13}C]-labeled reduced (GSH) and [4,5,6,7,8,10-^{13}C]-labeled oxidized glutathione (GSSG), indicating that glutamate, glycine, and/or cysteine were also synthesized from the lactate (Figure 5 and Table S2).

Purified hESC-Derived Cardiomyocytes Showed High Proliferative Capacity

We next investigated the proliferative capacity of mouse and human ESC-derived cardiomyocytes purified using metabolic selection. Some of the purified cardiomyocytes expressed Ki67 antigen (Figure 6A) and showed EdU-incorporation activities (Figure 6B). For directly assessing the rate of karyokinesis and cytokinesis after metabolic selection, the purified hESC-derived aggregates were completely dissociated and then seeded sparsely onto the MEF-layered dishes. Counting of immunocytochemically α-actinin-positive cells after 2, 4, 6, and 8 days revealed that the purified cardiomyocytes could proliferate up to 2.5-fold in 8 days, and the fraction of multinuclear cardiomyocytes increased over time compared with the second day (Figure 6C).

Purified Human PSC-derived Cardiomyocytes Showed Physiologically Relevant Action-Potential Configurations and Drug Responses

Action-potential recording using glass microelectrodes revealed that the purified hESC-derived cardiomyocytes had nodal- (14 of 76), atrial- (23 of 76), or ventricular-like (39 of 76) action potentials (Figure 6D and Figure S6A). We next evaluated their chronotropic response to the β-agonist isoproterenol and muscarinic agonist carbamylcholine using the multielectrode array (MEA) system; the former agent increased the beating frequency, whereas the latter decreased it, both in a dose-dependent manner (Figure 6E). We also found that beat frequency could be modulated by temperature (Figure S6B), and intracellular [Ca^{2+}] recording using Fluo-4 dye also revealed that the purified hESC-derived cardiomyocytes showed spontaneous and synchronized Ca^{2+} oscillations (Figure S6C).

Transplanted Purified Cardiomyocytes Did Not Form Tumors

Finally, for investigation of the potential tumorigenicity of the purified cardiomyocyte populations, 1,000 undifferentiated hESCs, 2.0×10^5 nonpurified hESC-derived cardiomyocytes, or the same number of purified cells were transplanted into the testes of immunocompromised nonobese diabetic severe combined immunodeficient (NOD-SCID) mice. Two months later, 9 of 10 (90%), 8 of 20 (40%), and 0 of 20 mice developed tumors, respectively (Figure 6F and Figure S6D). For further verification of the absence of residual undifferentiated cells, nonpurified and purified dispersed hESC-derived cells (2.0×10^5) were cultured on MEFs under PSC maintenance culture conditions (colony formation assay) for 4 days. Nonpurified hESC-derived cells formed Oct3/4- or Tra1-60-positive piled-up colonies, but

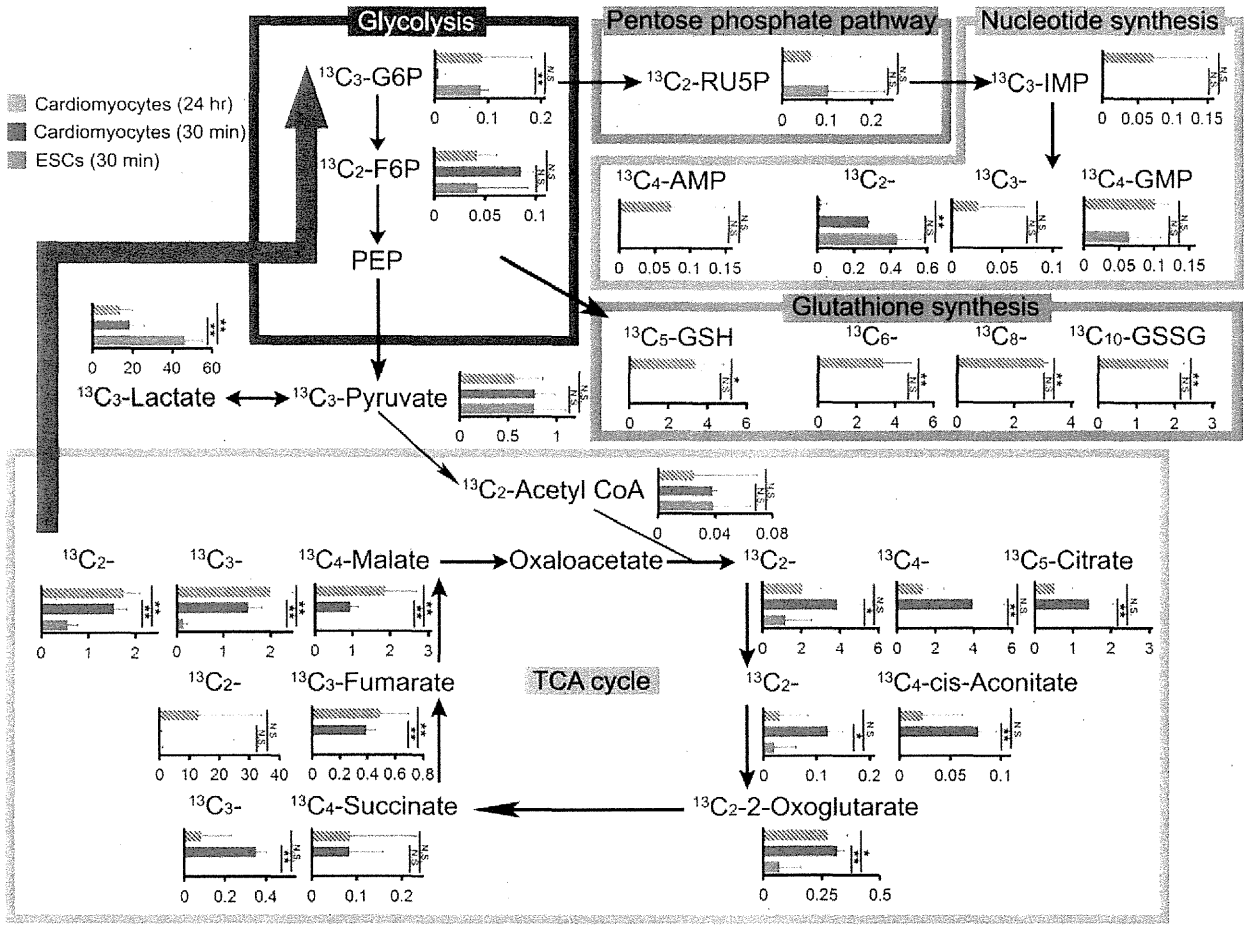

Figure 5. Mechanisms Underlying the Lactate-Mediated Survival of Cardiomyocytes

Fluxome analysis of the short-term (30 min) and long-term (24 hr) administration of [^{13}C]-labeled lactate under glucose-depleted conditions in neonatal cardiomyocytes and ESCs (ESCs, n = 4; cardiomyocytes, n = 3). The relationships between the kinds of bars, kinds of cell, and labeling conditions are shown in the upper left. All data were obtained from independent experiments. The bold red arrow on the right indicates a possible reflux pathway from malate to G6P. All units are nmol per 1.0 × 10^7 cells. *$p < 0.05$; **$p < 0.01$. Data are shown as mean ± SD. PEP, phosphoenolpyruvate. See also Figure S5 and Table S2.

the purified cardiomyocytes formed no colonies (Figure 6G and Figure S6E). To demonstrate the PSC-elimination capacity of the lactate method, we used a commercially available kit based on magnetic-beads-activated cell sorting with a Tra1-60 antibody. This experiment confirmed the apparent superiority of the lactate method in eliminating stem cells compared to the tested method (Figure S6F).

DISCUSSION

There are several approaches available for obtaining enriched cardiomyocyte populations from human PSCs. Ma et al. (2011) performed genetic-modification-based purification of cardiomyocytes (achieving >98% cardiomyocyte purity) from hiPSC derivatives, using the intrinsic *MYH6* gene to express a blasticidin S resistance gene. Dubois et al. (2011) used a surface protein, signal-regulatory protein alpha (SIRPA), as a cardiac-specific marker in hiPSC derivatives prepared through a highly cardiogenic differentiation procedure. They purified cardiomyocytes (up to 98% purity) via FACS from sources comprising 40%–50% cardiomyocytes. The method we report here is a simple medium-exchanging procedure that enabled cardiomyocyte purification of up to 99% from a cell source comprising only 10% cardiomyocytes, with an estimated recovery of cardiomyocytes of 74.4 ± 12.1%, based on direct cell count before and after purification. Previously we reported a mitochondrial method for purifying cardiomyocytes to >99% purity via FACS. Our direct comparison of these two methods revealed a higher cardiomyocyte-yield-based efficiency for the lactate method than for the mitochondrial method. The lactate method has quantitative and economic advantages relative to other existing cardiomyocyte-purification methods by virtue of its simplicity and ease of application.

One question that arose from our studies is why ESCs die within a few hours under the lactate method but cardiomyocytes survive for much longer, even though both cell types use lactate

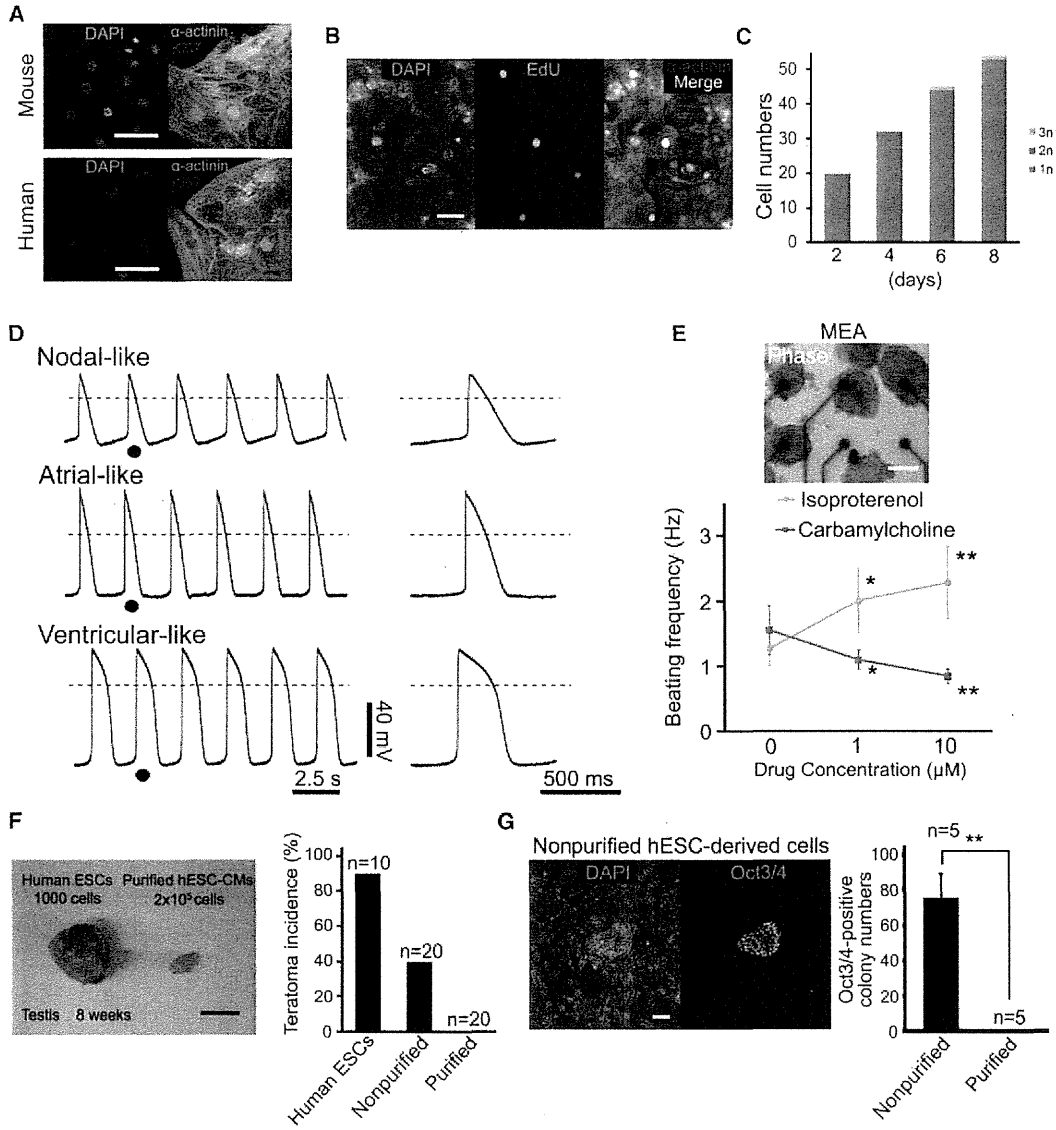

Figure 6. Characterization of ESC-Derived Cardiomyocytes after Metabolic Selection

(A) Immunofluorescent staining for α-actinin (green) and Ki67 (red) in the purified mouse (top) and human (bottom) ESC-CMs.

(B) EdU-positive cells (green) in purified hESC-CMs.

(C) Numbers of hESC-derived dispersed cardiomyocytes after metabolic selection. The numbers of cardiomyocytes with single, double, and more than triple nuclei are separately represented by the blue, red, and green bars, respectively.

(D) Action-potential recording of the purified hESC-CMs using microelectrodes. Shown are representative configurations of the nodal- (top), atrial- (middle), and ventricular-like (bottom) action potentials.

(E) Drug responses in purified hESC-derived aggregates using the MEA system (top). The line graph (bottom) represents the chronotropic response against β-agonist isoproterenol (green; n = 3) and muscarinic agonist carbamylcholine (orange; n = 3). All data were obtained from independent experiments.

(F) The teratoma-forming capacities of hESCs (1,000 cells), nonpurified hESC-derived cells (2.0 × 10^5 cells), and purified hESC-CMs (2.0 × 10^5 cells) were evaluated through their transplantation into the testes of NOD-SCID mice. The bar graph represents the summarized results (hESCs, n = 10; nonpurified, n = 20; purified, n = 20).

(G) Immunofluorescent staining for Oct3/4 in dispersed cells from nonpurified hESC-derived EBs. The bar graph shows numbers of hESC-like colonies obtained from hESC-derived cells (2.0 × 10^5; n = 5).

Scale bars represent 50 μm (A and B), 100 μm (E and G), and 1 cm (F). *p < 0.05; **p < 0.01. Data are shown as mean ± SD. See also Figure S6.

for biomass synthesis. Through our investigations, we eliminated the possibility that lactate supplementation caused toxic extracellular or intracellular acidification. We propose that these differing properties may be a result of (1) the retrospective glycolytic pathway consuming two ATP molecules during conversion of a lactate molecule to G6P, and (2) ESCs not being

able to effectively obtain ATP from glycolysis nor from OXPHOS under glucose-depleted conditions. Therefore, activation of the retrospective glycolytic pathway may accelerate a catastrophic balance of ATP supply and demand in ESCs, whereas cardiomyocytes can maintain cellular ATP homeostasis by producing more ATP via a highly active OXPHOS mechanism (Hattori et al., 2010).

A patient would theoretically require about 10^9 cardiomyocytes in therapeutic applications of purified cardiomyocytes. In this study, we obtained approximately 5×10^5 purified human cardiomyocytes per 177 cm^2 dish. Taking into account their postpurification proliferative capacities, rough estimates therefore suggest that 1×10^9 cardiomyocytes could be obtained from 800 dishes (14.13 m^2). This scale is close to the capacity of commercially available automatic large-scale culture systems and suggests that combining more sophisticated differentiation methods with our lactate method could facilitate realistic application of PSC-derived cardiomyocytes to human therapy.

EXPERIMENTAL PROCEDURES

Animals

All animals including pregnant ICR mice, neonatal Wistar rats, and NOD-SCID mice (8 weeks old, male) were purchased from CLEA Japan (Tokyo). All experimental procedures and protocols were approved by the Animal Care and Use Committee of Keio University and conformed to the National Institutes of Health Guide for the Care and Use of Laboratory Animals.

Cells

Mouse ESCs were obtained from the Laboratory of Pluripotent Cell Studies, RIKEN Center for Developmental Biology. The hESC line (KhES-2 and KhES-3) was obtained from the Department of Development and Differentiation, Institute for Frontier Medical Sciences, Kyoto University and used in conformity with the Guidelines for Derivation and Utilization of Human Embryonic Stem Cells of the Ministry of Education, Culture, Sports, Science, and Technology, Japan. The hiPSC line (253G4 and 201B7) was obtained from the Center for iPSC Research and Application, Kyoto University. The skeletal myoblast cell line (C2C12), hepatocyte cell line (HepG2), and renal cell line (HEK293) were obtained from the American Type Culture Collection.

Reagents

The mouse monoclonal antibodies for α-actinin (immunoglobulin G_1 [IgG_1]) and Ki67 (IgM) were purchased from Sigma-Aldrich (Sigma). The mouse monoclonal antibodies for SMA (IgG_{2a}), βIII-tubulin, Oct3/4, and Tra1-60 were purchased from Dako, Promega, BD Transduction Laboratories, and Millipore, respectively. The goat polyclonal antibodies for GATA-4 (C-20) and Nkx2.5 (N-19) were purchased from Santa Cruz Biotechnology (Santa Cruz). Alexa Fluor 488 and 546 anti-mouse IgG (IgG_1, IgG_{2a}, and IgM) antibody and anti-goat IgG antibody were purchased from Invitrogen. DAPI and E-cadherin-Fc were also purchased from Invitrogen. Tetramethylrhodamine methyl ester perchlorate (TMRM), mitotracker red, 2′,7′-bis-(2-carboxyethyl)-5-(and-6)-carboxyfluorescein (BCECF) and Fluo-4 dye were purchased from Invitrogen. Fibronectin, isoproterenol hydrochloride, carbamylcholine, and α-CHC were purchased from Sigma. The [^{13}C]-labeled glucose and lactate were purchased from Isotec. The [^{14}C]-labeled lactate was purchased from PerkinElmer.

Maintenance of Mouse and Human PSCs

We maintained mouse ESCs on gelatin- or E-cadherin-coated dishes in Glasgow minimum essential medium (MEM) (Sigma) supplemented with 10% fetal bovine serum (FBS; Equitech-Bio), 0.1 mM MEM nonessential amino acid solution (Sigma), 2 mM L glutamine (Sigma), 0.1 mM β-mercaptoethanol (Sigma), and 2,000 U/ml murine leukemia inhibitory factor (Chemicon) (Nagaoka et al., 2006). We maintained hESCs and hiPSCs on MEFs in Dulbecco's modified Eagle's medium/nutrient mixture F-12 Ham 1:1 (DMEM-F12; Sigma) supplemented with 20% knockout serum replacement (Invitrogen), 0.1 mM MEM nonessential amino acid solution (Sigma), 2 mM L glutamine (Sigma), 0.1 mM β-mercaptoethanol (Sigma), and 4 ng/ml basic fibroblast growth factor (Wako).

Differentiation of Human PSC-Derived Cardiomyocytes

We cultured the enzymatically detached undifferentiated colonies of hESCs and hiPSCs with αMEM (Wako Pure Chemical, Wako) that contained 50 μg/ml ascorbic acid, supplemented with 5% FBS (Biowest) and 0.1 mM β-mercaptoethanol in bacterial Petri dishes for formation of EBs. EBs containing rhythmically beating cells were observed 14 to 20 days later. Typically, 1%–10% of EBs contained beating cells. Media were changed once a week. EBs were used for purification experiments between days 20 and 30.

Purification of hESC- and hiPSC-Derived Cardiomyocytes

The selection medium was prepared before use. Glucose-free DMEM (no glucose, no pyruvate; Invitrogen) supplemented with 4 mM lactate medium was produced using 1 M lactate stock solution prepared from diluting 10 M lactate (Wako Pure Chemical) with sterile 1M Na-HEPES (Sigma). The human PSC-derived EBs at differentiation day 20 to 30 were extensively washed with and exposed to the selection medium. Media were changed every 2 or 3 days for eliminating dead cells via rapid flushing using 40 μm filters (Becton Dickinson). Cells were sampled daily from day 6 of purification for optimizing the timing of harvest for each batch. We split sampled cells into two experiments: one for test cultivation and another for FACS analysis. In the test cultivation, cells were transferred to fibronectin-coated dishes and cultured for several days with αMEM supplemented with 5% FBS. FACS analysis was performed using α-actinin antibodies. Our criterion for determining the harvest day was at least 95% purity indicated by FACS analysis. All harvested cells were then transferred to fibronectin-coated dishes and cultured for several more days under αMEM supplemented with 5% FBS, during which the media were changed several times for complete removal of debris consisting of dead cells and insoluble matrix. The purified cardiomyocytes were finally collected by rapid flushing. Movies were recorded using a fluorescence microscope (BZ-9000; Keyence).

Cardiomyocyte Purification Using Mitochondrial Dye for Gene Array

To prepare purified cardiomyocytes for the gene array, we used hearts from neonatal mice (P1). Purification of mouse neonatal cardiomyocytes using mitochondrial TMRM dye was performed by FACS (FACS Aria; Becton Dickinson), as described previously (Hattori et al., 2010).

Immunofluorescence

We fixed cells with 4% paraformaldehyde in PBS (pH 7.0) for 20 min. Subsequently, cells were permeabilized with 0.1% Triton X-100 (Sigma) at room temperature for 10 min and then incubated with the primary antibody at 4°C overnight. Cells were then washed with Tris-buffered saline (TBS) containing 0.1% Tween 20 four times prior to incubation with the secondary antibodies at room temperature for 1 hr. After nuclear staining with DAPI (Invitrogen), stained cells were detected by fluorescence microscopy (IX71; Olympus) or confocal-laser microscopy (LSM 5 DUO; Carl Zeiss).

Cell Viability under Glucose-Depleted Conditions with or without Lactate

Neonatal cardiomyocytes, ESCs, and noncardiomyocytes including MEFs, HepG2, HEK293, peripheral lymphatic cells, C2C12, skeletal myotubes, and fetal neurons were exposed to glucose-free DMEM (Invitrogen) supplemented with or without lactate (Wako). Cell viabilities were determined by the LIVE/DEAD Viability/Cytotoxicity Assay Kit (Invitrogen) based on the simultaneous determination of live and dead cells with the calcein AM and ethidium homodimer-1 probes. Fluorescence imaging of the cells (live cells were labeled green, whereas the nuclei of dead cells were labeled red) was performed with fluorescence microscopy (IX70 microscope; Olympus) equipped with a color charge-coupled device camera (CS220; Olympus). The green-labeled live area was measured using Image J. Relative cell viabilities were calculated in percentages, compared with those before treatment.

FACS Analysis Using Sarcomeric α-Actinin Antibody

Purified cardiomyocytes were completely dissociated by 0.25% trypsin-EDTA and then fixed with 4% paraformaldehyde for 10 min. Subsequently, cells were permeabilized with 0.1% Triton X-100 (Sigma) at room temperature for 10 min and then incubated with the sarcomeric α-actinin antibody (Sigma) for 3 hr. Cells were washed with TBS containing 0.1% Tween 20 prior to incubation with the Alexa Fluor 488 donkey anti-mouse IgG secondary antibody (Invitrogen) at room temperature for 2 hr. These cells were analyzed via FACS (EPICS XL; Beckman Coulter).

Quantitative Real-Time PCR

Total RNA was extracted with ISOGEN reagent (Nippon Gene), and real-time PCR was performed as described previously (Yuasa et al., 2005). For quantitative analysis, complementary DNA (cDNA) was used as the template in a TaqMan real-time PCR assay using the ABI Prism 7700 sequence detection system (Applied Biosystems, Foster City, CA, USA) according to the manufacturer's instructions. Data were normalized to *GAPDH*. Human heart, skeletal muscle, and brain total RNA was purchased from Takara Bio. The primers and TaqMan probe for human *NANOG*, *POU5F1*, *ACTC1*, *NKX2.5*, *MYH6*, *MYOD*, *AFP*, *MAP2*, and *GAPDH* were Hs02387400_g1, Hs01895061_u1, Hs00606316_m1, Hs00231763_m1, Hs00411908_m1, Hs02330075_g1, Hs01040607_m1, Hs00258900_m1, and Hs02758991_g1, respectively.

Glucose Fluxome Analysis by Capillary Electrophoresis and Mass Spectrometry

In neonatal cardiomyocytes, ESCs, and noncardiomyocytes including HepG2 and C2C12, the media were switched to modified DMEM supplemented with 10% FBS and 10 mM [^{13}C]-labeled glucose (Isotec) instead of 10 mM glucose. In 30 min, these cells were washed in 10% mannitol (Wako) and then plunged into methanol that contained internal standards (300 μM each of methionine sulfone for cations and MES for anions). Cells and the medium were collected for capillary electrophoresis and mass spectrometry experiments using an Agilent capillary electrophoresis system equipped with an air pressure pump, an Agilent 1100 series mass selective detector mass spectrometer, an Agilent 1100 series isocratic high-performance liquid-chromatography pump, a G1603A Agilent capillary electrophoresis and mass spectrometry adaptor kit, and a G1607A Agilent capillary electrophoresis and mass spectrometry sprayer kit (Agilent Technologies) as described previously (Endo et al., 2009; Shintani et al., 2009). Values were corrected against cell numbers.

Lactate Fluxome Analysis by Capillary Electrophoresis and Mass Spectrometry

In mouse ESCs, hESC-derived EBs, MEFs, and neonatal rat cardiomyocytes, the medium was switched to modified glucose-free DMEM (Invitrogen) supplemented with 4 mM [^{13}C]-labeled lactate (Isotec). After 30 min and/or 24 hr, these cells were collected for analysis as described above. Values were corrected against cell numbers.

Action-Potential Recordings Using Microelectrodes

The microscope was equipped with a recording chamber and a noise-free heating plate (Micro Warm Plate; Kitazato Supply). Standard glass microelectrodes that had a DC resistance of 25–35 mega Ω when filled with pipette solution (2 M KCl) were positioned using a motor-driven micromanipulator (EMM-3SV; Narishige) under optical control. Spontaneously contracting hESC-derived aggregates after metabolic selection were seeded and cultured in fibronectin-coated dishes, and the action potentials were recorded. The recording pipette was connected to a patch-clamp amplifier (Axopatch 200B; Axon Instruments), and the signal was passed through a low-pass filter with a cutoff frequency of 2 kHz and digitized using an A/D converter with a sampling frequency of 10 kHz (Digidata 1440A; Axon Instruments). Signals were monitored, recorded as electronic files, and then analyzed offline with pCLAMP 10 software (Axon Instruments).

Field-Potential Recordings Using the MEA System

To characterize the functional properties of our purified human PSC-derived cardiomyocytes, we performed extracellular recording of field potentials using the MEA system (Multi Channel Systems, Reutlingen, Germany) as described previously (Tanaka et al., 2009; Zwi et al., 2009). To assess the effects of different drugs on the electrophysiological properties, drug-diluted medium was applied to the MEA culture plate. The applied drugs included isoproterenol hydrochloride and carbamylcholine. The temperature was maintained at 37°C during these recordings. For further evaluation of the effects of temperature on the electrophysiological properties, temperatures were also varied from 30°C to 42°C.

Teratoma Formation

To verify the elimination of immature cells with the potential to form teratomas by purification, we transplanted 2.0 × 10^5 purified hESC-derived cardiomyocytes, 2.0 × 10^5 nonpurified hESC-derived cells, and 1,000 undifferentiated hESCs into the testes of immunocompromised NOD-SCID mice. Two months after transplantation, animals were euthanized, and teratoma incidence was evaluated.

Colony-Formation Assay

Nonpurified and purified hESC-derived cells (2.0 × 10^5) were completely dissociated and cultured on the MEFs with PSC maintenance culture condition with 10 μM of ROCK inhibitor for 4 days. Then, immunofluorescence staining for Oct3/4 and Tra1-60 was performed, and colony numbers were counted.

ATP Measurement

Cells were plated onto gelatin-coated 96-well white, clear-bottom culture plates (Costar). After 2 days, cells were treated with the glucose-free plus lactate medium for a given length of time. ATP levels were measured using an ATP assay kit (Toyo Ink). In brief, 100 μl of the lysis and assay solution provided by the manufacturer was added to the wells. After shaking for 1 min and incubating for 20 min at 23°C, we measured luminescence of an aliquot of the solution in a luminometer (Synergy 4; BioTek).

[^{14}C]-Labeled Lactate Uptake

After washing the plates in glucose-free medium, cells were exposed to the glucose-free plus 1 μM [^{14}C]-labeled lactate condition. After 30 min, the cells were washed three times in fresh medium and collected for analysis. [^{14}C] signal was detected by liquid scintillation analysis (Packard). Values were corrected against cell number.

EdU Incorporation Assay

In one case, purified hESC-derived cardiomyocytes were dispersed and seeded in the MEF precultured dishes and cultured with αMEM containing 5% FBS for 12 hr for attachment. They were then treated with 10 μM EdU for 48 hr and processed according to the manufacturer's instructions (Invitrogen, Click-iT EdU Alexa Fluor 488 kit). The cells then underwent additional immunofluorescent staining for α-actinin and were observed by fluorescence microscopy. In another experimental setting, the intact floating hESC-derived EBs were treated with 10 μM EdU for 48 hr, dispersed, and then fixed with 4% paraformaldehyde followed by FACS analysis for determining the percentage of EdU-incorporated cells.

Statistical Analysis

All statistical analyses were performed using the Statistical Package for the Social Sciences for Windows version 17 software (SPSS, Chicago). Values are presented as mean ± SD. The statistical significance was evaluated using Student's t tests. A p value of less than 0.05 was considered statistically significant.

SUPPLEMENTAL INFORMATION

Supplemental Information includes six figures, two tables, three movies, and Supplemental Experimental Procedures and can be found with this article online at http://dx.doi.org/10.1016/j.stem.2012.09.013.

ACKNOWLEDGMENTS

We thank K. Sekine in the Department of Anatomy, Keio University School of Medicine for technical assistance with primary culturing of neurons. This study was mainly supported by the Strategic Funds for the Promotion of Science and Technology of the Japanese Ministry of Education Sports, Science, and

Technology (MEXT) and the Highway Program for the Realization of Regenerative Medicine and partially supported by a Japan Heart Foundation research grant, the Japan Science and Technology Agency (JST), Exploratory Research for Advanced Technology (ERATO), Suematsu Gas Biology Project, and a research grant from Asubio Pharma. F.H., T.T., and M.Y. are the employees and H.Y. is an indirect employee of Asubio Pharma Co., Ltd.

Received: July 31, 2011
Revised: May 10, 2012
Accepted: September 13, 2012
Published online: November 15, 2012

REFERENCES

Ashburner, M., Ball, C.A., Blake, J.A., Botstein, D., Butler, H., Cherry, J.M., Davis, A.P., Dolinski, K., Dwight, S.S., Eppig, J.T., et al.; The Gene Ontology Consortium. (2000). Gene ontology: tool for the unification of biology. Nat. Genet. *25*, 25–29.

Burd, L.I., Jones, M.D., Jr., Simmons, M.A., Makowski, E.L., Meschia, G., and Battaglia, F.C. (1975). Placental production and foetal utilisation of lactate and pyruvate. Nature *254*, 710–711.

Burridge, P.W., Keller, G., Gold, J.D., and Wu, J.C. (2012). Production of de novo cardiomyocytes: human pluripotent stem cell differentiation and direct reprogramming. Cell Stem Cell *10*, 16–28.

Clément, S., Stouffs, M., Bettiol, E., Kampf, S., Krause, K.H., Chaponnier, C., and Jaconi, M. (2007). Expression and function of alpha-smooth muscle actin during embryonic-stem-cell-derived cardiomyocyte differentiation. J. Cell Sci. *120*, 229–238.

Dubois, N.C., Craft, A.M., Sharma, P., Elliott, D.A., Stanley, E.G., Elefanty, A.G., Gramolini, A., and Keller, G. (2011). SIRPA is a specific cell-surface marker for isolating cardiomyocytes derived from human pluripotent stem cells. Nat. Biotechnol. *29*, 1011–1018.

Endo, J., Sano, M., Katayama, T., Hishiki, T., Shinmura, K., Morizane, S., Matsuhashi, T., Katsumata, Y., Zhang, Y., Ito, H., et al. (2009). Metabolic remodeling induced by mitochondrial aldehyde stress stimulates tolerance to oxidative stress in the heart. Circ. Res. *105*, 1118–1127.

Fijnvandraat, A.C., van Ginneken, A.C., Schumacher, C.A., Boheler, K.R., Lekanne Deprez, R.H., Christoffels, V.M., and Moorman, A.F. (2003). Cardiomyocytes purified from differentiated embryonic stem cells exhibit characteristics of early chamber myocardium. J. Mol. Cell. Cardiol. *35*, 1461–1472.

Fisher, D.J., Heymann, M.A., and Rudolph, A.M. (1981). Myocardial consumption of oxygen and carbohydrates in newborn sheep. Pediatr. Res. *15*, 843–846.

Gassanov, N., Er, F., Zagidullin, N., and Hoppe, U.C. (2004). Endothelin induces differentiation of ANP-EGFP expressing embryonic stem cells towards a pacemaker phenotype. FASEB J. *18*, 1710–1712.

Hashimoto, T., Hussien, R., and Brooks, G.A. (2006). Colocalization of MCT1, CD147, and LDH in mitochondrial inner membrane of L6 muscle cells: evidence of a mitochondrial lactate oxidation complex. Am. J. Physiol. Endocrinol. Metab. *290*, E1237–E1244.

Hattori, F., and Fukuda, K. (2012). Strategies for replacing myocytes with induced pluripotent stem in clinical protocols. Transplant Rev. (Orlando) *26*, 223–232.

Hattori, F., Chen, H., Yamashita, H., Tohyama, S., Satoh, Y.S., Yuasa, S., Li, W., Yamakawa, H., Tanaka, T., Onitsuka, T., et al. (2010). Nongenetic method for purifying stem cell-derived cardiomyocytes. Nat. Methods *7*, 61–66.

Hidaka, K., Lee, J.K., Kim, H.S., Ihm, C.H., Iio, A., Ogawa, M., Nishikawa, S., Kodama, I., and Morisaki, T. (2003). Chamber-specific differentiation of Nkx2.5-positive cardiac precursor cells from murine embryonic stem cells. FASEB J. *17*, 740–742.

Kinoshita, A., Tsukada, K., Soga, T., Hishiki, T., Ueno, Y., Nakayama, Y., Tomita, M., and Suematsu, M. (2007). Roles of hemoglobin Allostery in hypoxia-induced metabolic alterations in erythrocytes: simulation and its verification by metabolome analysis. J. Biol. Chem. *282*, 10731–10741.

Klug, M.G., Soonpaa, M.H., Koh, G.Y., and Field, L.J. (1996). Genetically selected cardiomyocytes from differentiating embronic stem cells form stable intracardiac grafts. J. Clin. Invest. *98*, 216–224.

Laflamme, M.A., Chen, K.Y., Naumova, A.V., Muskheli, V., Fugate, J.A., Dupras, S.K., Reinecke, H., Xu, C., Hassanipour, M., Police, S., et al. (2007). Cardiomyocytes derived from human embryonic stem cells in pro-survival factors enhance function of infarcted rat hearts. Nat. Biotechnol. *25*, 1015–1024.

Ma, J., Guo, L., Fiene, S.J., Anson, B.D., Thomson, J.A., Kamp, T.J., Kolaja, K.L., Swanson, B.J., and January, C.T. (2011). High purity human-induced pluripotent stem cell-derived cardiomyocytes: electrophysiological properties of action potentials and ionic currents. Am. J. Physiol. Heart Circ. Physiol. *301*, H2006–H2017.

Nagaoka, M., Koshimizu, U., Yuasa, S., Hattori, F., Chen, H., Tanaka, T., Okabe, M., Fukuda, K., and Akaike, T. (2006). E-cadherin-coated plates maintain pluripotent ES cells without colony formation. PLoS ONE *1*, e15.

Neely, J.R., and Morgan, H.E. (1974). Relationship between carbohydrate and lipid metabolism and the energy balance of heart muscle. Annu. Rev. Physiol. *36*, 413–459.

Passier, R., van Laake, L.W., and Mummery, C.L. (2008). Stem-cell-based therapy and lessons from the heart. Nature *453*, 322–329.

Shintani, T., Iwabuchi, T., Soga, T., Kato, Y., Yamamoto, T., Takano, N., Hishiki, T., Ueno, Y., Ikeda, S., Sakuragawa, T., et al. (2009). Cystathionine beta-synthase as a carbon monoxide-sensitive regulator of bile excretion. Hepatology *49*, 141–150.

Sonveaux, P., Végran, F., Schroeder, T., Wergin, M.C., Verrax, J., Rabbani, Z.N., De Saedeleer, C.J., Kennedy, K.M., Diepart, C., Jordan, B.F., et al. (2008). Targeting lactate-fueled respiration selectively kills hypoxic tumor cells in mice. J. Clin. Invest. *118*, 3930–3942.

Takahashi, K., Tanabe, K., Ohnuki, M., Narita, M., Ichisaka, T., Tomoda, K., and Yamanaka, S. (2007). Induction of pluripotent stem cells from adult human fibroblasts by defined factors. Cell *131*, 861–872.

Tanaka, T., Tohyama, S., Murata, M., Nomura, F., Kaneko, T., Chen, H., Hattori, F., Egashira, T., Seki, T., Ohno, Y., et al. (2009). In vitro pharmacologic testing using human induced pluripotent stem cell-derived cardiomyocytes. Biochem. Biophys. Res. Commun. *385*, 497–502.

Thomson, J.A., Itskovitz-Eldor, J., Shapiro, S.S., Waknitz, M.A., Swiergiel, J.J., Marshall, V.S., and Jones, J.M. (1998). Embryonic stem cell lines derived from human blastocysts. Science *282*, 1145–1147.

Uosaki, H., Fukushima, H., Takeuchi, A., Matsuoka, S., Nakatsuji, N., Yamanaka, S., and Yamashita, J.K. (2011). Efficient and scalable purification of cardiomyocytes from human embryonic and induced pluripotent stem cells by VCAM1 surface expression. PLoS ONE *6*, e23657.

Werner, J.C., and Sicard, R.E. (1987). Lactate metabolism of isolated, perfused fetal, and newborn pig hearts. Pediatr. Res. *22*, 552–556.

Xu, C., He, J.Q., Kamp, T.J., Police, S., Hao, X., O'Sullivan, C., Carpenter, M.K., Lebkowski, J., and Gold, J.D. (2006). Human embryonic stem cell-derived cardiomyocytes can be maintained in defined medium without serum. Stem Cells Dev. *15*, 931–941.

Yuasa, S., Itabashi, Y., Koshimizu, U., Tanaka, T., Sugimura, K., Kinoshita, M., Hattori, F., Fukami, S., Shimazaki, T., Ogawa, S., et al. (2005). Transient inhibition of BMP signaling by Noggin induces cardiomyocyte differentiation of mouse embryonic stem cells. Nat. Biotechnol. *23*, 607–611.

Zwi, L., Caspi, O., Arbel, G., Huber, I., Gepstein, A., Park, I.H., and Gepstein, L. (2009). Cardiomyocyte differentiation of human induced pluripotent stem cells. Circulation *120*, 1513–1523.

Laboratory Investigation (2012) 92, 1766–1776

Impaired post-infarction cardiac remodeling in chronic kidney disease is due to excessive renin release

Masahito Ogawa[1,2,3], Jun-ichi Suzuki[2], Kiyoshi Takayama[4], Takaaki Senbonmatsu[5], Yasunobu Hirata[2,6], Ryozo Nagai[6] and Mitsuaki Isobe[1]

The complex pathophysiological interactions between heart and kidney diseases are collectively known as cardiorenal syndrome. The renin–angiotensin system (RAS) may have a pivotal role in the development of cardiorenal syndrome. The aim of this study was to elucidate the RAS activity responsible for adverse post-infarction remodeling and prognosis in mice with renal failure. To establish the type IV cardiorenal syndrome model, 5/6 nephrectomy (NTX) was performed in a surgical procedure, followed by the induction of myocardial ischemia (MI) by a coronary artery ligation 4 weeks later. NTX and MI resulted in deteriorated left ventricular remodeling and RAS activation, which was improved by an aliskiren that appeared to be independent of renal function and blood pressure (BP). Moreover, MI induced in renin and angiotensinogen double-transgenic (Tg) mice showed comparable effects to MI plus NTX mice, including advanced ventricular remodeling and enhancement of RAS, oxidative stress, and monocytes chemoattractant protein (MCP)-1. Aliskiren suppressed these changes in the MI-induced Tg mice. In *in vitro* study, Nox2 expression was elevated by the stimulation of plasma from NTX mice in isolated neonatal cardiomyocytes. However, Nox2 upregulation was negated when we administered plasma from aliskiren-treated-NTX mice or isolated cardiomyocytes from AT1-deficient mice. Primary mononuclear cells also showed an upregulation in the expression of Nox2 and MCP-1 by stimulation with plasma from NTX mice. Our data suggest that renal disorder results in ventricular dysfunction and deteriorates remodeling after MI through excessive RAS activation. Moreover, renin inhibition improved the changes caused by cardiorenal syndrome.
Laboratory Investigation (2012) **92,** 1766–1776; doi:10.1038/labinvest.2012.136; published online 17 September 2012

KEYWORDS: infarction; inflammation; remodeling; renin angiotensin system

It is well known that there is a complex relationship between cardiovascular and renal diseases. In fact, end-stage renal disease or decreased estimated glomerular filtration rate correlates with an increased risk of cardiovascular diseases.[1] This clinical condition is known as cardiorenal syndrome. In addition, the presence of chronic kidney disease (CKD) is a relatively frequent complication in patients with advanced heart failure and left ventricular (LV) dysfunction. Its presence is associated with a worse prognosis following cardiovascular diseases.[2] Although preventing this condition includes identification and amelioration of the precipitating factors and connections,[3] the pathophysiological mechanisms of the syndrome remain to be elucidated. It is also known that the presence of CKD increases severity, worsens the response to treatment, and is associated with poor cardiac and renal outcomes in cardiorenal syndrome.[4,5]

The renin–angiotensin system (RAS) has a critical role in the development of cardiovascular and renal disease in a clinical setting. It has been reported that the role of RAS in congestive heart failure (CHF) and CKD is complex owing to involvement of multiple peptides and receptors. Increased RAS activity results in the development of CHF by stimulation of cardiac hypertrophy, apoptosis, and LV dilatation. Although RAS mediates the development of cardiorenal syndrome, clinical studies indicate that angiotensin receptor blockers do not reduce cardiovascular events in patients with nephropathy.[6]

Aliskiren, a new class of the first representative non-peptide direct renin inhibitor,[7] is broadly used as an antihypertensive

[1]Department of Cardiovascular Medicine, Tokyo Medical and Dental University, Tokyo, Japan; [2]Departments of Advanced Clinical Science and Therapeutics, Tokyo, Japan; [3]Research Fellow of the Japan Society for the Promotion of Science, Tokyo, Japan; [4]NB Health Laboratory, Tokyo, Japan; [5]Department of Pharmacology, Saitama Medical University, Tokyo, Japan and [6]Cardiovascular Medicine, University of Tokyo, Tokyo, Japan
Correspondence: Dr J-i Suzuki, MD, PhD, Departments of Advanced Clinical Science and Therapeutics, University of Tokyo, Tokyo Medical and Dental University, 7-3-1 Hongo, Bunkyo, Tokyo 113-8655, Japan.
E-mail: junichisuzuki-circ@umin.ac.jp

Received 13 April 2012; revised 9 July 2012; accepted 1 August 2012

drug, as its effects directly suppress the plasma concentration of Ang peptides.[8,9] Recent papers reveal the benefit of aliskiren following myocardial ischemia (MI) independent of pressor effects in rodent and human studies.[10,11] RAS activity during sleep time, which is independent of systemic pressure, has important role in the progression of cardiac remodeling. The half-life of aliskiren is very long (24–48 h) compared with an ACE inhibitor (about 6 h). Aliskiren treatment would inhibit the RAS activity independent of systemic pressure because of its longevity. A clinical trial (ALTITUDE) in type 2 diabetes using cardiorenal endpoints is ongoing,[12,13] but the detailed pathophysiological roles of aliskiren have not yet been elucidated in the experimental models of cardiorenal syndrome.

Thus, the aim of this study was to elucidate the RAS activity responsible for adverse myocardial remodeling with renal failure and to clarify the effect of aliskiren on this condition. In this study, we demonstrated that renal disorder results in ventricular dysfunction and deteriorates remodeling after MI through excessive RAS activation in this cardiorenal model. Aliskiren treatment suppressed cardiac dysfunction, LV remodeling, and inflammatory or oxidative factors compared with the vehicle-treated group. These results may be a new methodological approach against prognosis in patients with renal failure suffering acute-MI.

MATERIALS AND METHODS

Animals

Male C57BL/6 mice were obtained from Crea, Japan. Transgenic (Tg) mice were generated using heterozygotes carrying either the 15-kb *human renin* gene with the 3-kb native promoter or the 14-kb *human angiotensinogen* gene with the 1.3-kb promoter. Double-Tg mice were created by cross-mating between *human renin*-Tg and *human angiotensinogen*-Tg mice. Both mice were backcrossed to the C57Bl/6 background. Human renin in *renin*-Tg mice is found at ~34-fold higher concentration than that obtained from normal human plasma. Plasma Ang II concentration and plasma renin activity (PRA) are ~3.5-fold and 6–9-fold higher in double-Tg mice than in wild-type (WT) mice.[14] *Human renin*-Tg mice and *human angiotensinogen*-Tg mice were provided by RIKEN BRC (Tsukuba, Japan). *AT1*$^{-/-}$ mice were also used as described previously.[15]

Experimental Protocols

All mice were 6–8 weeks of age when the experiment started. A murine model of 5/6 nephrectomy (NTX) was generated by a two-step surgical procedure as described previously.[16] Two to three arterial branches of the left kidney were ligated leaving an intact kidney segment. The right kidney was removed, and the mice received 0.9% NaCl in their drinking water. Four weeks after NTX, MI was induced by ligation of the left anterior descending (LAD) coronary artery, and this was continued for 28 days[17] (Supplementary Figure 1). Double-Tg and WT-mice were induced MI without NTX. We killed the mice on day 7 ($n = 8$–10 per each group) and day 28 ($n = 17$–22 per each group). In total, 4–6 mice in each assay, and 7–11 mice in pathological analysis were randomly picked from each group (Supplementary Figure 1).

These experiments conform to the Guide for the Care and Use of Laboratory Animals in the Tokyo Medical and Dental University, University of Tokyo.

Treatment Protocols

Animals were assigned randomly into treatment groups and were administered a subcutaneous injection of aliskiren (25 mg/kg; Novartis Pharma), hydralazine (in drinking water, 30 mg/kg), apocynin (in drinking water, 150 mg/kg; Sigma-Aldrich), or a vehicle (PBS; Supplementary Figure 1). These drugs were administered daily for 8 weeks after NTX. The aliskiren and apocynin dosage were decided based on previously papers.[8,18] The dose of hydralazine was determined to show the equal effect of decreasing BP comparable with the aliskiren-treated group.

Physiological Examinations

Heart rate and BP (systolic pressure) were measured in conscious mice by using a tail-cuff system (BP-98A, Softron, Tokyo, Japan). Transthoracic echocardiography was performed with ultrasound equipment (Nemio, Toshiba, Tokyo, Japan) using a 14-MHz annular array transducer. Hearts were imaged in the two-dimensional mode in short-axis views at the level of papillary muscle. EF were calculated as $EF = SV/EDV \times 100$; $SV = EDV - ESV$; $EDV = (7 \times LVDd^3/1000)/\{2.4 + (LVDd/10)\}$; $ESV = (7 \times LVDs^3/1000)/\{2.4 + (LVDs/10)\}$.

Histological Analysis

Harvested hearts were quickly dipped into 4% paraformaldehyde. The hearts were embedded in paraffin. Sample sections (1 μm) of the tissue were stained by Mallory and viewed using a light microscope with a computer-assisted analyzer (Image Pro Express software).[19] To demonstrate remodeling analysis, infarct size, infarct thickness, infarct length, LV circumference, and septal thickness were measured with the computer-assisted analyzer. Collagen production was identified by the Sirius Red, and the area of collagen was determined in the LV border area. To avoid bias, the histologist was single blinded to the treatment groups of mice.

Hydroxyproline Assay

Collagen concentrations of whole hearts were measured using the hydroxyproline assay 1 week after MI operation. The homogenated samples in acetic buffer were hydrolyzed. Chloramine T buffer were added to sample and incubated for 20 min. Erhlich's solution was then added to each sample, and incubated for 20 min. Absorbance 550 nm was read on a microplate reader.[20]

Real-Time (RT) PCR

mRNA of whole hearts were collected using the TRIzol method 1 week after MI or 4 weeks after NTX. RT-PCR was performed to determine the mRNA expression of ANP (assay ID: Mm01255747_g1), monocytes chemoattractant protein (MCP)-1 (Mm00441242_m1), collagen-type I (Mm0130243_g1), AT1a (Mm00558224_s1), NADPH oxidase (Nox)2 (Mm1287742_m1), and Nox4 (Mm00479246_m1). The mRNA expression of the target gene was normalized to *18s ribosomal RNA* (4308329). Quantitative data were calculated to normalize the control group as baseline using the comparative CT ($\Delta\Delta$CT) method.[21]

Immunohistochemistry

Immunohistochemistry (IHC) was performed using a primary antibody against renin (no. 593), followed by the Nichirei Simple stain kit (Nichirei).[19] Immunological changes were scored on a 0 to 5 basis (no detected to large quantity detected) by single-blinded histologists.

Plasma Biochemistry

Blood was collected in heparinized microtubes and subjected to centrifugation. Plasma creatinine levels were measured using the enzymatic method by SRL.

PRA Analysis

Plasma was collected from mice and diluted in an Ang I generation buffer containing 0.1 M phosphate buffer, 5 mM EDTA, and 1 mM PMSF. The mixtures were incubated for 30 min. Ang I expression was measured using the Ang I EIA kit (Peninsula Laboratories). Quantitative data were obtained to determine endogenous Ang I in each group by the following equation: quantitative data = Ang I value–endogenous Ang I value.

Cell Preparation and Culture

The hearts were isolated from neonatal mice (1–2-day-old), and minced with PBS. The hearts were then denatured by collagenase (Roche diagnosis). Isolated cells were plated for 40 min. Fibroblasts adhered to the plate, while cardiomyocytes did not. Cardiomyocytes were cultured in MEM medium containing 5% FBS on 3.5-mm plane plastic dishes. Fibroblasts were cultured in DMEM (containing 10% FBS) until confluent. Mononuclear cells were collected from the spleens using cell strainers and were plated in RPMI1640 medium.[19] Isolated cardiomyocytes or mononuclear cells were serum staved, and stimulated by murine plasma (5% in the medium) isolated from NTX, aliskiren-treated NTX on week 4, or non-NTX mice as a control. Aliskiren or vehicle (PBS) was administrated to the medium for 30 min before plasma stimulation.

Statistical Analysis

All data are expressed as mean ± s.e.m. A survival analysis was performed using the Kaplan–Meier method with the log-rank test. Data were compared and differences between the two groups were analyzed by the *t*-test. Differences in data between multiple groups were subjected to one-way or two-way ANOVA and Bonferroni post-test. A statistical test was performed using the Prism. Differences with values of $P<0.05$ were considered significant.

RESULTS

Aliskiren Suppressed NTX-Induced Hypertension

NTX resulted in hypertension compared with the non-NTX mice 2 weeks after the operation. Although aliskiren reduced systolic BP, hydralazine administration resulted in a decline in BP comparable to aliskiren administration (Figure 1a).

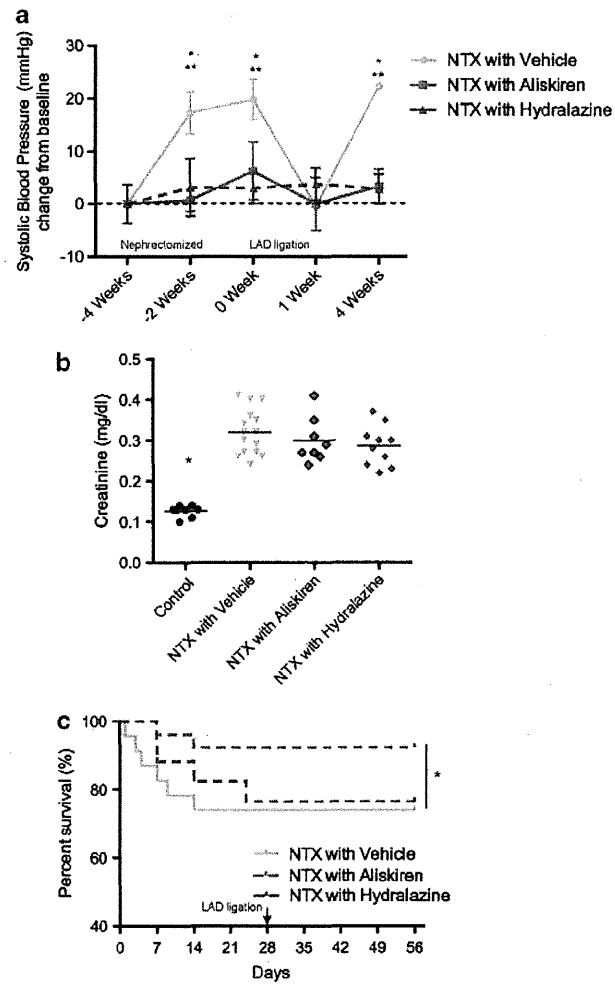

Figure 1 Aliskiren suppressed 5/6 nephrectomy (NTX)-induced hypertension. (**a**) Representative data of blood pressure in NTX mice. Mice were administrated vehicle (dilute blue line; $n=10$), aliskiren (red line; $n=8$), or hydralazine (blue line; $n=10$). $^{*}P<0.05$ *vs* aliskiren, $^{**}P<0.05$ *vs* hydralazine. (**b**) Representative data of serum creatinine levels in NTX. Plasma creatinine levels are shown 4 weeks after NTX in NTX and non-NTX groups ($P<0.05$). $^{*}P<0.05$ *vs* each group. (**c**) Representative data of survival rate in NTX. Vehicle: $n=26$; aliskiren: $n=24$; hydralazine: $n=13$, $^{*}P<0.05$.

Plasma creatinine levels were elevated 4 weeks after NTX compared with the non-NTX group. Neither aliskiren nor hydralazine administration changed the plasma creatinine levels (Figure 1b).

Although many control mice died within the first 4 weeks after NTX (73.91%, $n=24$), aliskiren administration significantly improved the survival rates of mice with NTX (percent survival = 92.31%, $n=26$; $P<0.05$ *vs* vehicle). However, mice treated with hydralazine showed survival rates comparable to those of vehicle-treated mice (76.92%, $n=13$; Figure 1c).

NTX Augmented Renin Expression and Activity

To investigate whether NTX activated renin expression and activity, we performed IHC and plasma biochemistry analysis. Four weeks post NTX, the remaining kidneys showed increased renin expression (4.5 ± 0.3, $P<0.05$) at the juxtaglomerular area compared with the non-NTX kidneys (1.0 ± 0.4; Figures 2a and b). Although NTX elevated PRA compared with the control mice, aliskiren treatment negated this effect (Figure 2c). Hydralazine treatment did not alter the PRA value. Although cardiac *AT1* transcription was elevated by nephrectomy compared with the control hearts (Figure 2d), aliskiren treatment did not change the level.

Aliskiren Suppressed MI plus NTX-induced Myocardial Remodeling

To clarify the relationship between renal disorder and cardiac dysfunction, we induced MI by LAD ligation in mice that had undergone NTX. Cardiac function was analyzed by echocardiogram and performed 1 and 4 weeks post LAD ligation (Table 1). MI-induced hearts showed myocardial infarction in large anterior region of LV. NTX had no effect on the LV ejection fraction (LVEF) of non-infarcted hearts ($86.0\% \pm 2.7\%$) compared with those that had not undergone NTX ($86.0\% \pm 1.0\%$). MI hearts with NTX showed increased impairment of LVEF (at 1 week: $51.6\% \pm 4.7\%$, 4 weeks: $36.4\% \pm 2.2\%$; $n=8$) compared with MI hearts without NTX (at 1 week: $70.7\% \pm 5.9\%$, 4 weeks: $53.8\% \pm 2.6\%$; $n=10$). However, aliskiren significantly improved LVEF of MI hearts with NTX (1 week: $67.5\% \pm 3.0\%$, 4 weeks: $65.4\% \pm 2.4\%$; $n=11$) compared with the vehicle. Hydralazine did not improve LVEF of MI hearts with NTX (1 week: $52.1\% \pm 3.0\%$, 4 weeks: $36.4\% \pm 2.2\%$; $n=7$; Figures 3a and b). Aliskiren treatment also significantly suppressed ratio of lung/body weight compared with the vehicle-treated group (Table 2).

LAD ligation resulted in significant pathological remodeling of the LV anterior wall 4 weeks after ischemia induction (Table 3). Infarction length and septal wall thickness were not

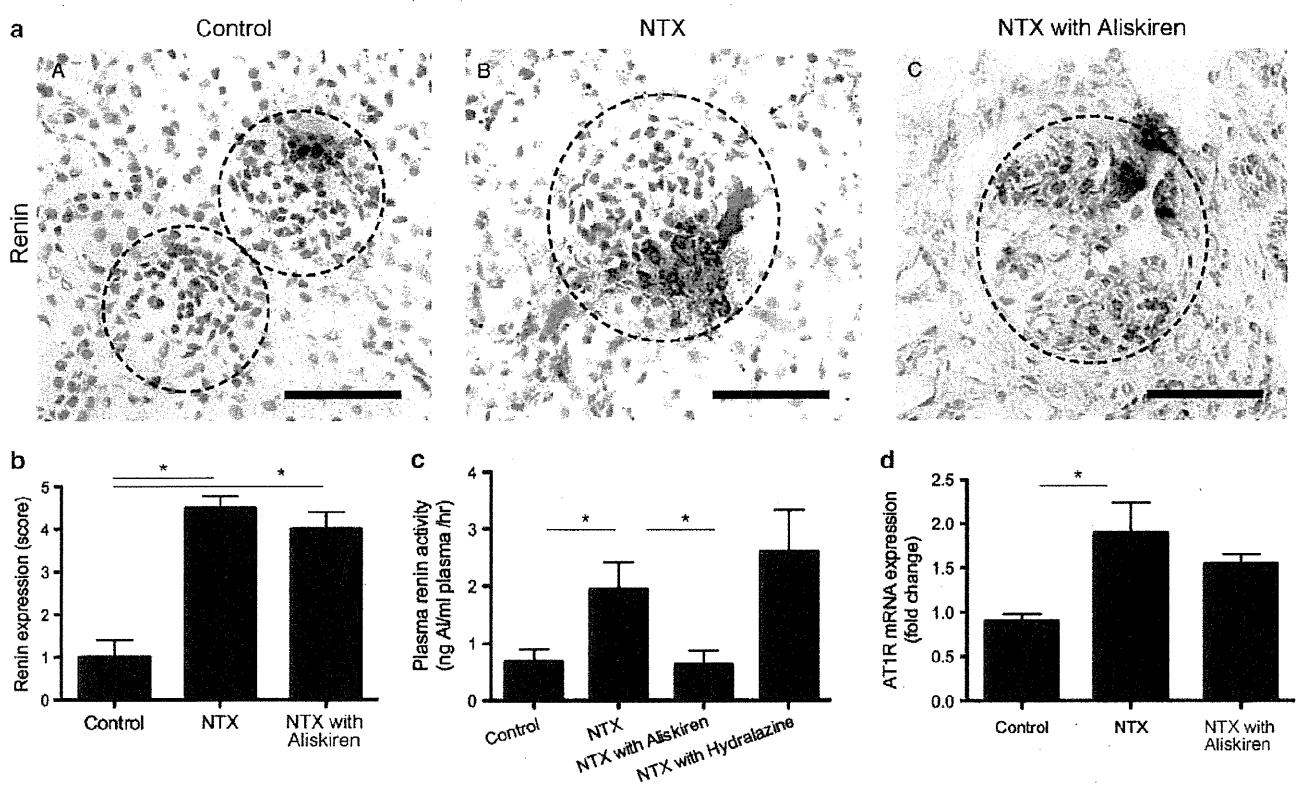

Figure 2 NTX (5/6 nephrectomy) augmented renin expression and activity. (**a**) Representative immunohistochemistry (IHC) of kidneys from NTX mice. Dot-line circle indicates glomerular area. Bar shows 50 μm. (**b**) Quantitative data of the IHC. *$P<0.05$. (**c**) Representative plasma renin activity in NTX mice. *$P<0.05$ (**d**) Representative Real-TimePCR of hearts from NTX mice. *$P<0.05$.

Table 1 Echocardiography and heart rate

(Weeks)	NTX-MI with Vehicle				NTX-MI with Aliskiren				NTX-MI with Hydralazine				MI alone			
	−4	0	1	4	−4	0	1	4	−4	0	1	4	−4	0	1	4
Atrial wall thickness (mm)	0.80 ± 0.04	0.81 ± 0.04	0.93 ± 0.09	0.73 ± 0.05	0.88 ± 0.07	0.78 ± 0.04	1.15 ± 0.04	0.89 ± 0.07	0.90 ± 0.02	0.78 ± 0.04	0.86 ± 0.11	0.74 ± 0.05	0.83 ± 0.07	-	1.00 ± 0.09	0.80 ± 0.06
LVDd (mm)	3.32 ± 0.15	3.68 ± 0.15	3.71 ± 0.09	4.19 ± 0.25	3.43 ± 0.18	3.40 ± 0.09	3.23 ± 0.17	3.50 ± 0.10*	3.35 ± 0.33	3.75 ± 0.11	3.51 ± 0.14	3.90 ± 0.22	3.07 ± 0.11	-	3.31 ± 0.09	3.89 ± 0.22
LVSd (mm)	1.65 ± 0.12	1.83 ± 0.12	2.71 ± 0.17	3.42 ± 0.29	1.80 ± 0.20	1.84 ± 0.13	2.23 ± 0.19	2.48 ± 0.11*	1.70 ± 0.27	1.87 ± 0.03	2.74 ± 0.16	3.24 ± 0.19	1.50 ± 0.04	-	2.15 ± 0.18	3.12 ± 0.21
EF (%)	87.17 ± 1.22	87.75 ± 1.22	51.57 ± 4.66	36.38 ± 2.20	85.50 ± 2.56	84.50 ± 3.05	67.55 ± 4.72*	65.36 ± 2.38*	87.00 ± 3.18	87.10 ± 0.73	52.14 ± 2.98	40.29 ± 2.99	86.00 ± 1.00	-	70.67 ± 5.90*	53.80 ± 2.62*
FS (%)	49.67 ± 1.48	50.75 ± 1.48	21.86 ± 2.67	13.88 ± 0.81	48.00 ± 3.17	49.63 ± 1.22	32.00 ± 3.12*	30.27 ± 1.62*	49.00 ± 3.94	49.5 ± 0.91	21.71 ± 1.60	15.86 ± 1.55	48.11 ± 1.22	-	34.83 ± 4.22*	23.00 ± 1.61*
Heart rate (per min)	572.16 ± 40.67	655.9 ± 18.52	585 ± 29.54	592.40 ± 0.10	576.50 ± 72.5	607.63 ± 13.27	638.5 ± 27.76	587.29 ± 18.81	619.50 ± 42.41	653.86 ± 25.93	747.40 ± 4.76	669.14 ± 4.74	512.75 ± 9.56	-	522.10 ± 6.17	526.33 ± 15.89

Abbreviations: EF, ejection fraction; FS, fractional shortening; LVDd, left ventricular end-diastolic diameter; LVSd, left ventricular end-systolic diameter; MI, myocardial ischemia; NTX, 5/6 nephrectomy.
*$P<0.05$ *vs* NTX-MI with vehicle.

significantly different between the vehicle- and aliskiren-treated group. Although vehicle-treated LAD ligation resulted in LV thinning, aliskiren administration significantly reduced this pathological change. Enlarged LV circumference was also reduced by aliskiren. Collagen expression was significantly enhanced along the border by MI with NTX (19.3% ± 2.4%; $n=8$), but this was reduced by aliskiren administration (6.8% ± 2.0%; $n=11$; $P<0.05$; Figure 3c and Table 3). mRNA and collagen were collected from the cardiac ventricle on week 1 post MI. Although MI hearts elevated collagen-type I mRNA levels and collagen concentration compared with the hearts of control mice, MI with NTX hearts showed enhanced collagen levels compared with MI hearts without NTX (Figures 3d and e). Aliskiren suppressed the levels of collagen in MI hearts with NTX.

NTX Enhanced *ANP*, Oxidative Stress, and *MCP-1* in MI Mice

RAS is known to have a key role in myocardial hypertrophy and fibrosis via increased oxidative stress and the expression of inflammatory chemokines. Thus, we examined the levels of *ANP, Nox2, Nox4,* and *MCP-1* mRNA in MI or non-MI hearts treated by NTX. mRNA was collected from the cardiac ventricle 1 week after MI. *ANP* levels were elevated in the MI hearts compared with the non-MI hearts. Moreover, hearts with MI treated by NTX showed enhanced *ANP* mRNA levels compared with the MI hearts without NTX. The mRNA levels of *Nox2* and *Nox4* were elevated in MI hearts compared with non-MI hearts. Nox2 and Nox4 are isoforms of Nox, a major enzyme that produces reactive oxygen species (ROS). In addition, MI-induced hearts treated with NTX showed further elevation of *Nox2*, *Nox4,* and *MCP-1* mRNA levels as compared with the MI hearts that were not treated with NTX (Figures 4a–d). Aliskiren treatment significantly suppressed these levels compared with the NTX plus MI group.

It is known that Nox enzymes can be activated by RAS. To reveal the role of Nox enzymes in MI-induced myocardial remodeling in renal dysfunction, we administrated apocynin as a Nox inhibitor to the NTX plus MI mice. Although apocynin did not alter BP, attenuation of Nox improved LVEF and myocardial fibrosis in the 28 days after LAD ligation mice as compared with the vehicle-treated group (Figures 4e and f).

Double-Tg Mice Deteriorated After MI

Although we demonstrated that NTX deteriorated LV dysfunction through RAS activation, we did not clarify the relationship between upregulated circulating RAS and the progression of LV remodeling. To clarify the pathophysiological mechanism, we used human renin and angiotensinogen Tg mice. Systolic BP was consistently elevated in the double-Tg mice compared with the WT mice (Supplementary Figure 2A). The high BP resulted in mild cardiac

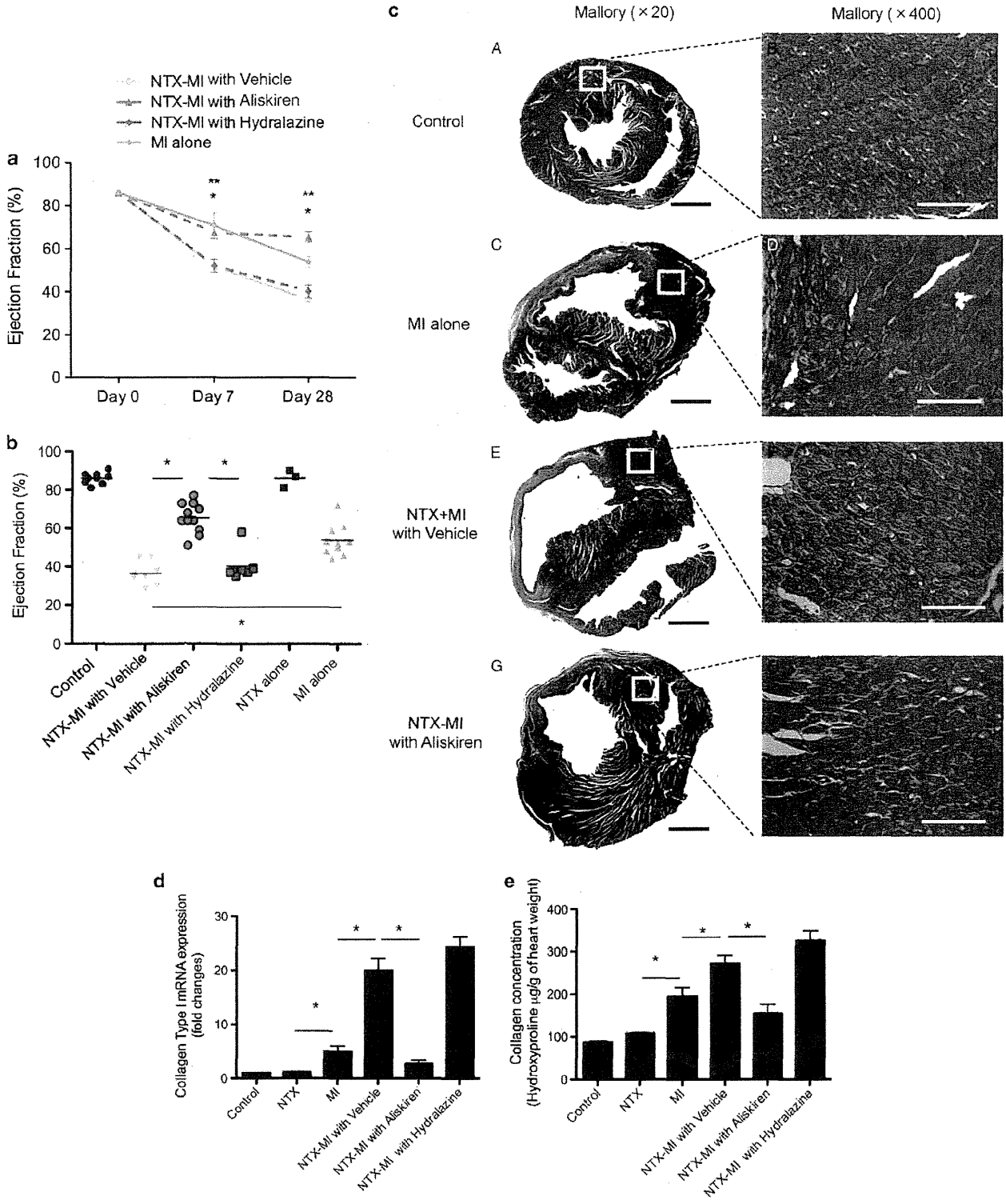

Figure 3 Aliskiren suppressed myocardial ischemia (MI) plus 5/6 nephrectomy (NTX)-induced myocardial remodeling. (**a**) Representative chronological observation of left ventricular ejection fraction (LVEF) in MI hearts with NTX (vehicle: $n=8$; aliskiren: $n=11$; and hydralazine: $n=7$). $^*P<0.05$ *vs* vehicle and hydralazine. (**b**) Representative LVEF data 28 days after MI. (**c**) Representative light micrograph of MI heart with NTX. Black bar shows 2 mm and white bar shows 50 μm. (**d**) Representative collagen-type I analysis in hearts in MI with NTX mice using real-time PCR (NTX: $n=4$; MI: $n=4$; NTX-MI: $n=6$; NTX-MI-aliskiren: $n=6$; and NTX-MI-hydralazine: $n=4$). (**e**) Representative collagen concentration analysis in MI hearts with NTX (NTX: $n=4$; MI: $n=4$; NTX-MI: $n=6$; NTX-MI-aliskiren: $n=6$; NTX-MI-hydralazine: $n=6$). $^*P<0.05$.